Supporting Information

Exceptionally effective benzene/cyclohexane separation on a nitro-decorated metal-organic framework

Aleksandr A. Sapianik,*[a,b] Konstantin A. Kovalenko,[a,b] Denis G. Samsonenko,[a,b] Marina O. Barsukova,[a,b] Danil N. Dybtsev[a,b] and Vladimir P. Fedin[a,b]

[a] Nikolaev Institute of Inorganic Chemistry SB RAS, 3 Akad. Lavrentiev Av., 630090 Novosibirsk, Russia.

[b] Novosibirsk State University, 2 Pirogova st., 630090 Novosibirsk, Russia.

sapianik@niic.nsc.ru

General remarks

Commercial reagents (pyridine (>99%)) and solvents (acetone (99.99%), acetonitrile (99%), tetrahydrofuran (THF, 99.9%)) were used without additional purification. The starting complex $[Li_2Zn_2(piv)_6(py)_2]$ and then isoreticular MOFs $[Li_2Zn_2(R\text{-}bdc)_3(bpy)]$ were synthesized according to procedures described previously [1]. $[Li_2Zn_2(NO_2\text{-}bdc)_3(bpy)]{\cdot}C_6H_6$ (**$1\text{-}NO_2{\supset}C_6H_6$**) was obtained by immersing of as synthesized $[Li_2Zn_2(NO_2\text{-}bdc)_3(bpy)]$ into benzene for 3 days. Unless specified, all reagents for synthesis were obtained from commercial sources and were used as received. N, N-dimethylformamide (DMF, 99%) was treated over activated molecular sieves 3 Å. Powder X-ray diffraction data were obtained on a Shimadzu XRD 7000S diffractometer (Cu Kα radiation). The following parameters were used: 2θ step = 0.03°, counting time = 1.0−2.5 s, 2θ scan range = 3−30°. For compounds after vapor sorption measurements, the powder X-ray diffraction patterns are present in Figures S29, S31. ^1H NMR spectra were recorded on a Bruker Advance 500 spectrometer.

Crystallographic studies

Diffraction data for single-crystals **$1\text{-}NO_2{\supset}C_6H_6$** were collected at 100 K on the 'Belok' beamline (λ = 0.80246 Å, ϕ-scans) of the National Research Center 'Kurchatov Institute' (Moscow, Russian Federation) using a Rayonix SX165 CCD detector. The data were indexed, integrated, and scaled, absorption correction was applied using the XDS program package [2]. The structures were solved by dual space algorithm (SHELXT [3]) and refined by the full-matrix least-squares technique (SHELXL [4]) in the anisotropic approximation (except hydrogen atoms). Positions of hydrogen atoms of organic ligands were calculated geometrically and refined in the riding model. The crystallographic data and details of the structure refinements are summarized in Table S1. CCDC 1992869 contains the supplementary crystallographic data for this paper. These data can be obtained free of charge from The Cambridge Crystallographic Data Center at https://www.ccdc.cam.ac.uk/structures/.

Summarized position **A** occupancy was determined as 0.6 (0.3 + 0.3) and summarized position **B** occupancy was determined as 0.4 (0.2 + 0.2). The determined 1 benzene molecule per formula unit is lower than the found amount of benzene according to sorption experiments. It is a common feature for the determination of guest molecules occupancies by SCXRD analysis since their position in the crystal structure is not so rigid in comparison with the host framework. Also during the SXRD experiment it is hard to save all guest molecules inside the pores. Since at the time of installation of the crystal it is subject to the influence of the external atmosphere and room temperature, and during the XRD experiment it is blown with cooled nitrogen. Given these factors, a single crystal gradually loses guest molecules and one can almost never succeed in obtaining the maximum occupancy of the positions of guest molecules. In our case, the final formula with ≈ 2.5 benzene molecules was obtained according to elemental analysis, which is in good agreement with the sorption capacity.

Table S1. Crystal data and structure refinement for **1-NO_2⊃C_6H_6**

Identification code	**1-NO_2⊃C_6H_6**
Empirical formula	$C_{40}H_{23}Li_2N_5O_{18}Zn_2$
M, g/mol	1006.25
T, K	100
Crystal system	monoclinic
Space group	*C2/c*
a, Å	18.477(3)
b, Å	17.976(3)
c, Å	17.533(3)
β, deg.	117.21(2)
V, Å^3	5178.8(17)
Z	4
D(calcd), g/cm^3	1.291
μ, mm^{-1}	1.334
F(000)	2032
Crystal size, mm	0.10 × 0.05 × 0.05
θ range for data collection, deg.	1.87–30.99
Index ranges	$-23 \le h \le 23$, $-23 \le k \le 23$, $-22 \le l \le 19$
Reflections collected / independent	32084/ 5888
R_{int}	0.0589
Reflections with $I > 2\sigma(I)$	4915
Goodness-of-fit on F^2	1.040
Final *R* indices [$I > 2\sigma(I)$]	$R_1 = 0.0870$, $wR_2 = 0.2617$
R indices (all data)	$R_1 = 0.0958$, $wR_2 = 0.2702$
Largest diff. peak / hole, *e*/Å^3	1.435/ -1.154

Vapor Sorption Experiments at 293 K

As synthesized [$Li_2Zn_2(R\text{-}bdc)_3(bpy)$] compounds were activated with the already described procedure [1]. The porosity was proved by measuring the N_2 adsorption isotherms and comparing with published results. Then samples were used for vapor sorption experiments. Benzene and cyclohexane adsorption isotherm measurements were carried out volumetrically on Quantochrome's Autosorb iQ equipped with thermostat TERMEX Cryo-VT-12 to adjust the temperature with 0.1 K accuracy. Adsorption−desorption isotherms were measured within the range of pressures of 1 to 75.3 torr for benzene and 77.1 torrs for cyclohexane which are corresponded to saturated pressures (P_0) at 293 K. The database of the National Institute of Standards and Technology [5] was used as a source of p−V−T relations at experimental pressures and temperature.

Adsorption isotherms

Adsorption isotherms were measured volumetrically at 293 K (Figure S1). Compounds with relatively large channel windows demonstrate fully reversible Type I isotherms with negligible adsorption-desorption hysteresis. Thus, benzene adsorption isotherms on compounds **1-H**, **1-Br,** and **1-NH$_2$** are reversible without hysteresis which is characterized for microporous compounds. Adsorption capacities of benzene (Table S2) are in a good agreement with pore volumes and the ordering is **1-H** > **1-NH$_2$** > **1-NO$_2$** ≈ **1-Br**.

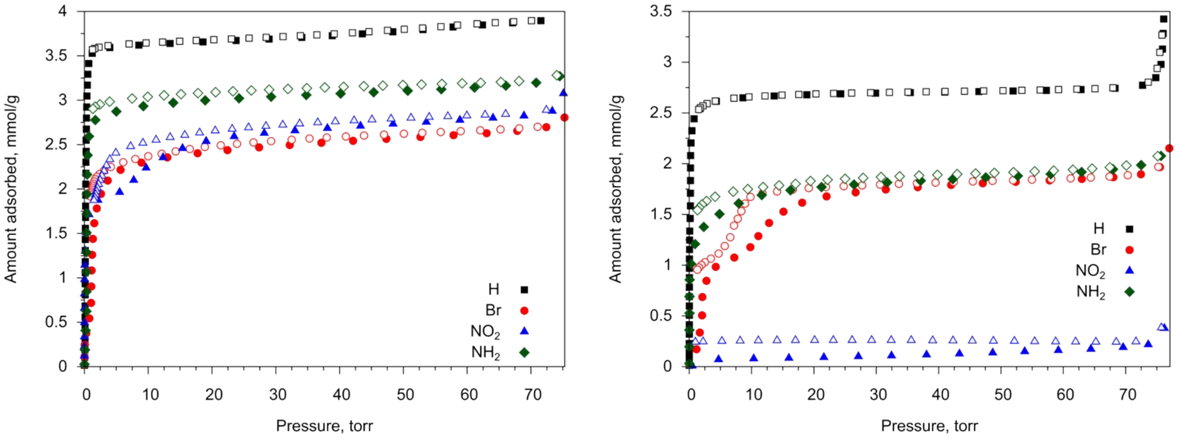

Figure S1. Benzene (left) and cyclohexane (right) sorption isotherms 293 K

Cyclohexane has slightly larger molecular sizes than benzene. Minimal projection radii are 3.64 Å and 3.46 Å correspondingly. Consequently, the reversible cyclohexane adsorption isotherms are observed only for **1-H** and **1-NH$_2$**, while the cyclohexane adsorption on **1-Br** has stepped character with hysteresis loop, and only limited adsorption (less than 0.25 mmol/g) on **1-NO$_2$**. The ordering of adsorption capacities at saturation conditions is **1-H** > **1-NH$_2$** ≈ **1-Br** >> **1-NO$_2$**.

Table S2. Uptakes of benzene and cyclohexane at 293 K in different units.

Compound	**benzene**		**cyclohexane**	
	mmol/g	**wt. %**	**mmol/g**	**wt. %**
1-H	3.9	30.4	2.8	23.3
1-Br	2.7	21.9	2.0	16.5
1-NO$_2$	2.9	22.5	0.2	1.8
1-NH$_2$	3.2	24.5	2.0	16.7

IAST calculations

For IAST calculations adsorption isotherms were fitted by the most appropriate model. Fittings were performed for isotherms in wt. %–torr units, so parameters are in the corresponding units.

Table S3. Fitted parameters for adsorption isotherms at 293 K.

	benzene	**cyclohexane**
1-H	Sum of Henry and Langmuir-Freundlich model $k = 0.0394$ $w = 27.6$ $b = 70.9$ $t = 0.391$	Langmuir model $w = 22.7$ $b = 11.9$
1-Br	Sum of Henry and Langmuir-Freundlich model $k = 0.0471$ $w = 17.7$ $b = 0.634$ $t = 0.395$	Dual-Site Langmuir-Freundlich model $w_1 = 7.74$ $b_1 = 0.000876$ $t_1 = 0.362$ $w_2 = 7.81$ $b_2 = 0.0241$ $t_2 = 0.171$
1-NO$_2$	Dual-Site Langmuir-Freundlich model $w_1 = 9.89$ $b_1 = 0.0537$ $t_1 = 0.815$ $w_2 = 13.0$ $b_2 = 38.5$ $t_2 = 0.994$	Henry isotherm $k = 0.0247$
1-NH$_2$	Sum of Henry and Langmuir-Freundlich model $k = 0.0471$ $w = 22.0$ $b = 398$ $t = 0.177$	Langmuir-Freundlich isotherm $w = 17.1$ $b = 1.54$ $t = 2.00$

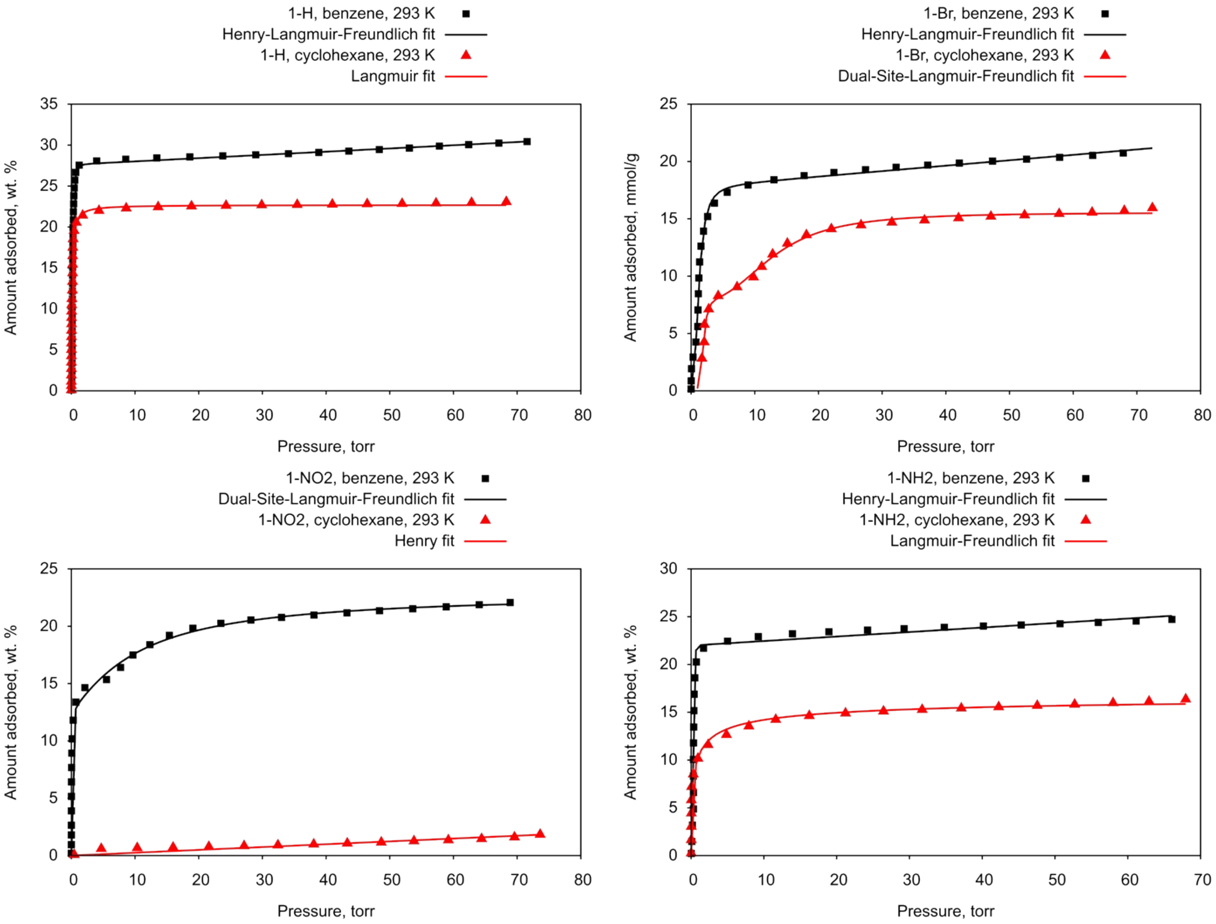

Figure S2. Isotherm fits.

The relationship between *P*, y_i and x_i (*P* — the total pressure of the gas phase, y_i — mole fraction of the *i*-component in the gas phase, x_i — mole fraction of the *i*-component in the absorbed state) is defined according to the IAST theory [6]:

$$\int_{p=0}^{p=\frac{Py_1}{x_1}} n_1(p)dlnp = \int_{p=0}^{p=\frac{Py_2}{x_2}} n_2(p)dlnp \tag{1}$$

The selectivity factors were determined as:

$$S = \frac{y_2 x_2}{y_1 x_1} = \frac{x_1(1-y_1)}{y_1(1-x_1)} \tag{2}$$

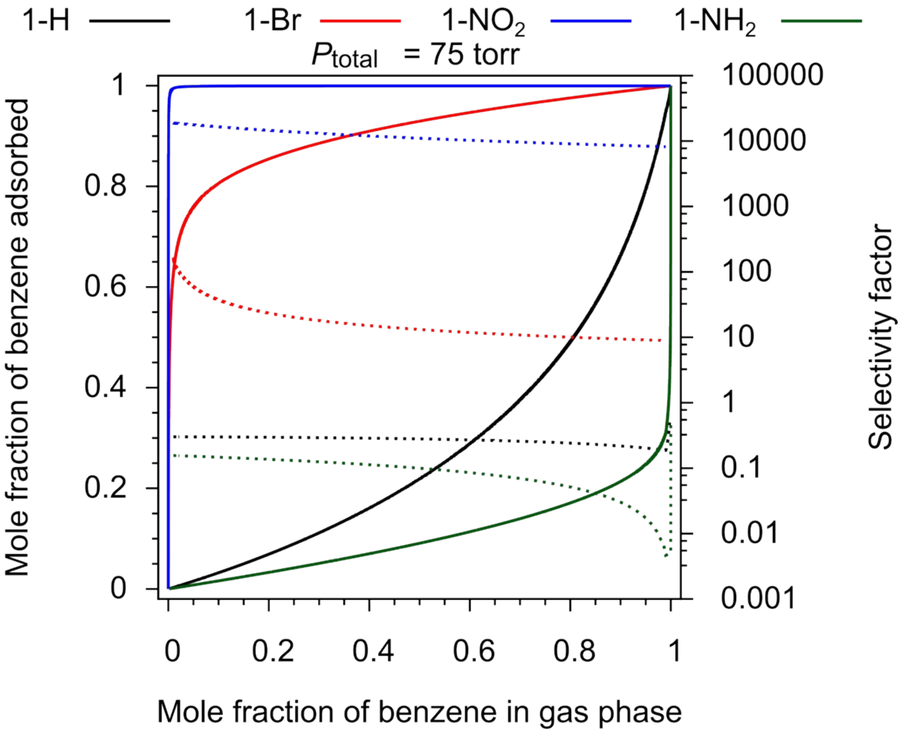

Figure S3. Dependence of mole fraction of benzene adsorbed (left scale, straight lines) and selectivity factors (right log scale, dotted lines) from initial benzene mole fraction in the vapor phase.

Vapour and liquid mixture separation

Sorption from a vapor phase. Before sorption, activation of samples of **1-NO$_2$** was performed. As synthesized **1-NO$_2$** was immersed in 10 ml of acetone for 3 days. Each day the crystals were decanted, and a new portion of acetone was added. Then the crystals were decanted and dried in vacuum at 50°C. Activated crystals (0.100 g) was placed in an open vial, which, in its turn, was immersed into a bigger vial containing a benzene-cyclohexane mixture with a given molar composition (9:1; 3:1; 1:1; 1:3; 1:9), closed with a cap. Then we used two different approaches to extract absorbed hydrocarbons - total MOF decomposition using KOH DMF solution and DMF assisted extraction. For two tested systems (9:1; 1:1) no critical difference between both methods was found (Figure S8-S11). Found benzene:cyclohexane ratios were **93.1:6.9** for decomposition process and **94.4:5.6** for extraction (for initially equimolar mixture). Found weight % for cyclohexane was 1.0% for decomposition and 0.90% for extraction (equimolar mixtures, calculated from DMF as internal standard) which is definitely the same value taking into account the errors of the method. As long as that simple DMF extraction was used for any further experiment since this approach does not destroy MOF structure. The amount and ratios between adsorbed hydrocarbons were calculated from ^{1}H-NMR spectra, given amounts of DMF-d$_7$were used as the internal standard. Calibration spectra are shown on Figure S4-S7. The ratio of benzene and cyclohexane in the mixture was determined by the ratio of the integrals of the peaks corresponding to benzene (7.4 ppm) and cyclohexane (1.4 ppm), taking into account the number of protons. Optimal exposure time to benzene:cyclohexane vapors were found in series of experiments including 20, 50, 150, 1440 minutes (Figures S12-S15), for further experiments at different compositions 50 minutes exposure time was used since even after 20 minutes no significant differences were found. We have checked the cyclicality for three cycles for equimolar initial benzene:cyclohexane mixture. After each cycle the additional acetone treatment and activation under vacuum while heating was carried out. Benzene cyclohexane ratio was found from ^{1}H-NMR spectra of DMF: DMF-d$_7$ solution which was used to fully extract these hydrocarbons from pores (Figures S15-S17). Found selectivities are shown in Table S4. Then 9:1, 3:1, 1:3, 1:9 molar mixtures of benzene:cyclohexane were tested (Figure S18-S21).

Sorption from a liquid phase. 0.100 g of **1-NO$_2$** was placed in a closed vial containing 2 ml of a benzene-cyclohexane mixture with given molar composition for 1 day. Then the crystals were very quickly filtered, washed with two portions of 2 ml of DMF, transferred in a vial for DMF assisted extraction for 1 day. After filtration given amounts of the filtrate were mixed with a given amount of DMF-d$_7$, and an ^{1}H NMR spectrum of a mixture was recorded (Figures S22-S26).

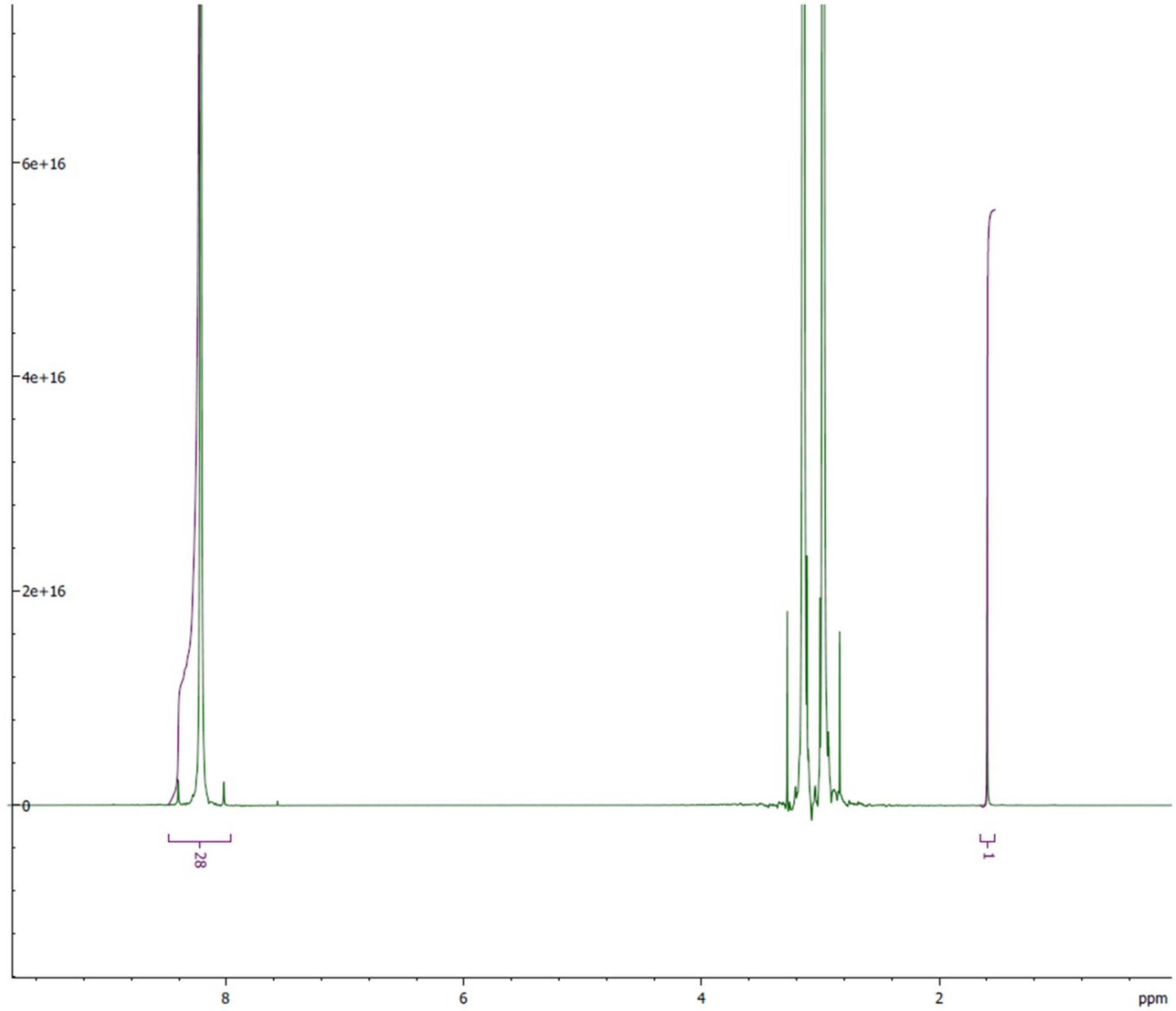

Figure S4. ^{1}H NMR spectrum of a calibration mixture of liquid phase containing 10 µl of cyclohexane in dimethylformamide/ dimethylformamide-d$_7$.

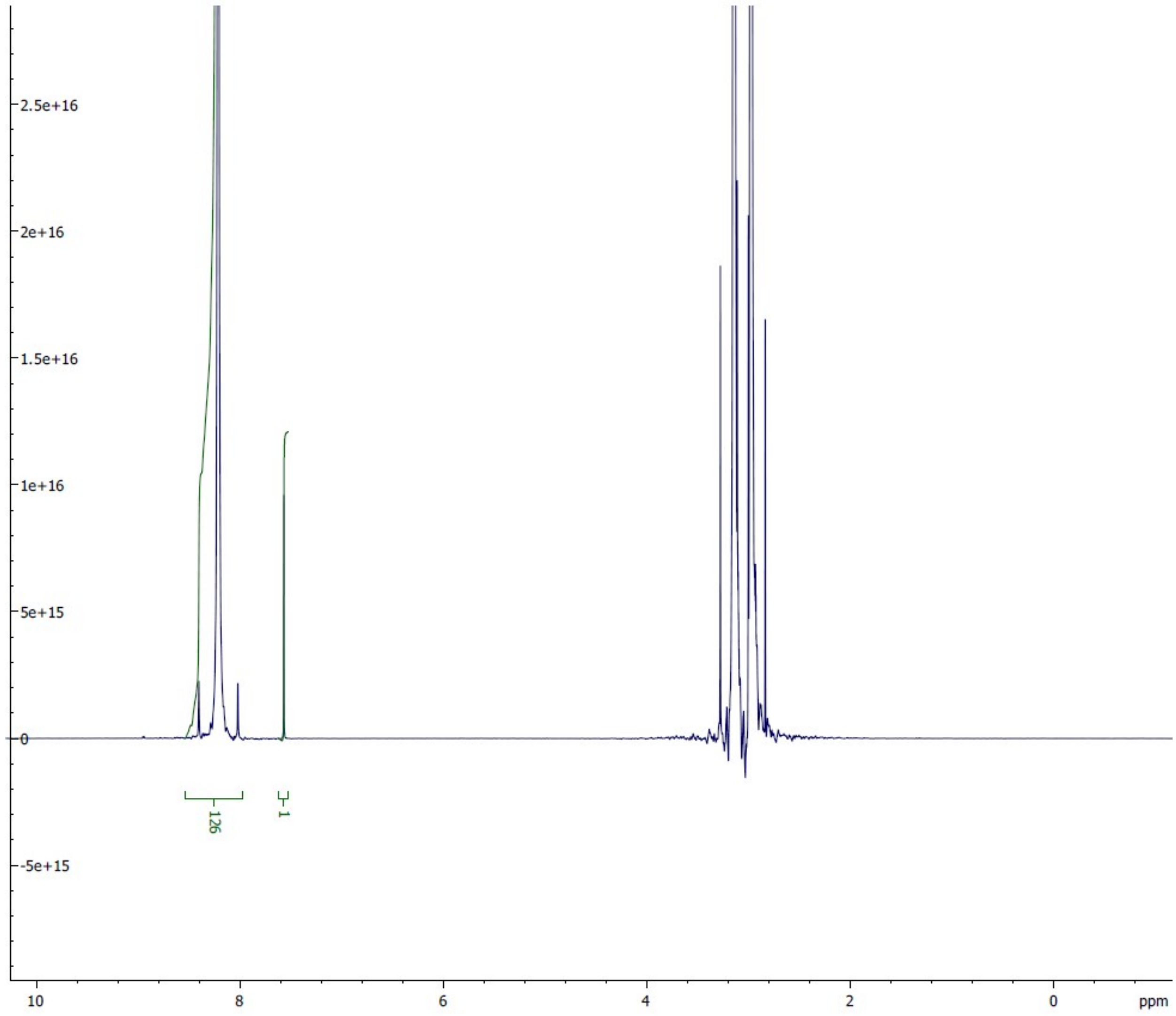

Figure S5. ^{1}H NMR spectrum of a calibration mixture of liquid phase containing 10 µl of benzene in dimethylformamide/ dimethylformamide-d$_7$.

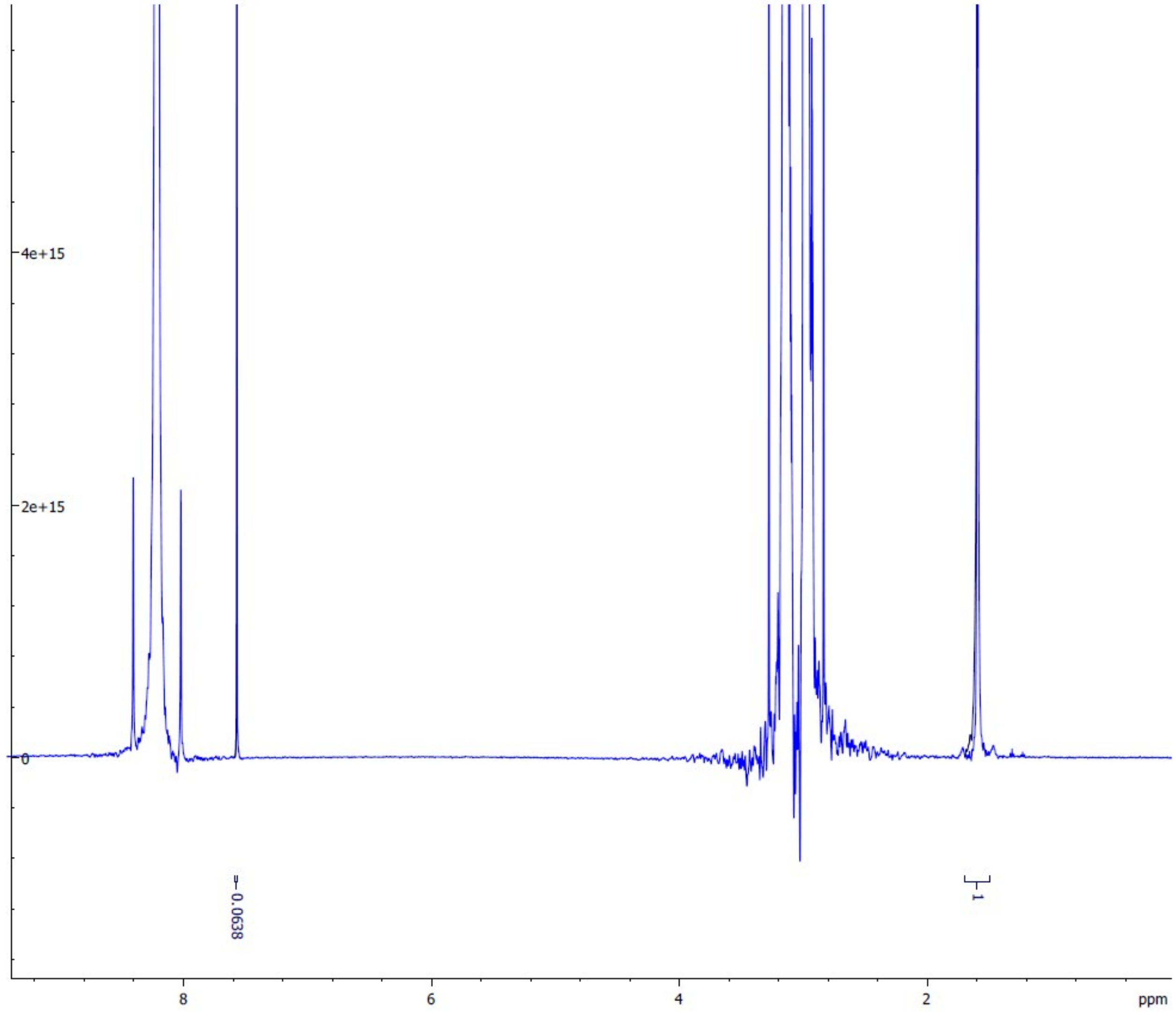

Figure S6. ^{1}H NMR spectrum of a calibration mixture of liquid phase containing 1 µl of benzene and 10 µl of cyclohexane in dimethylformamide/ dimethylformamide-d_7.

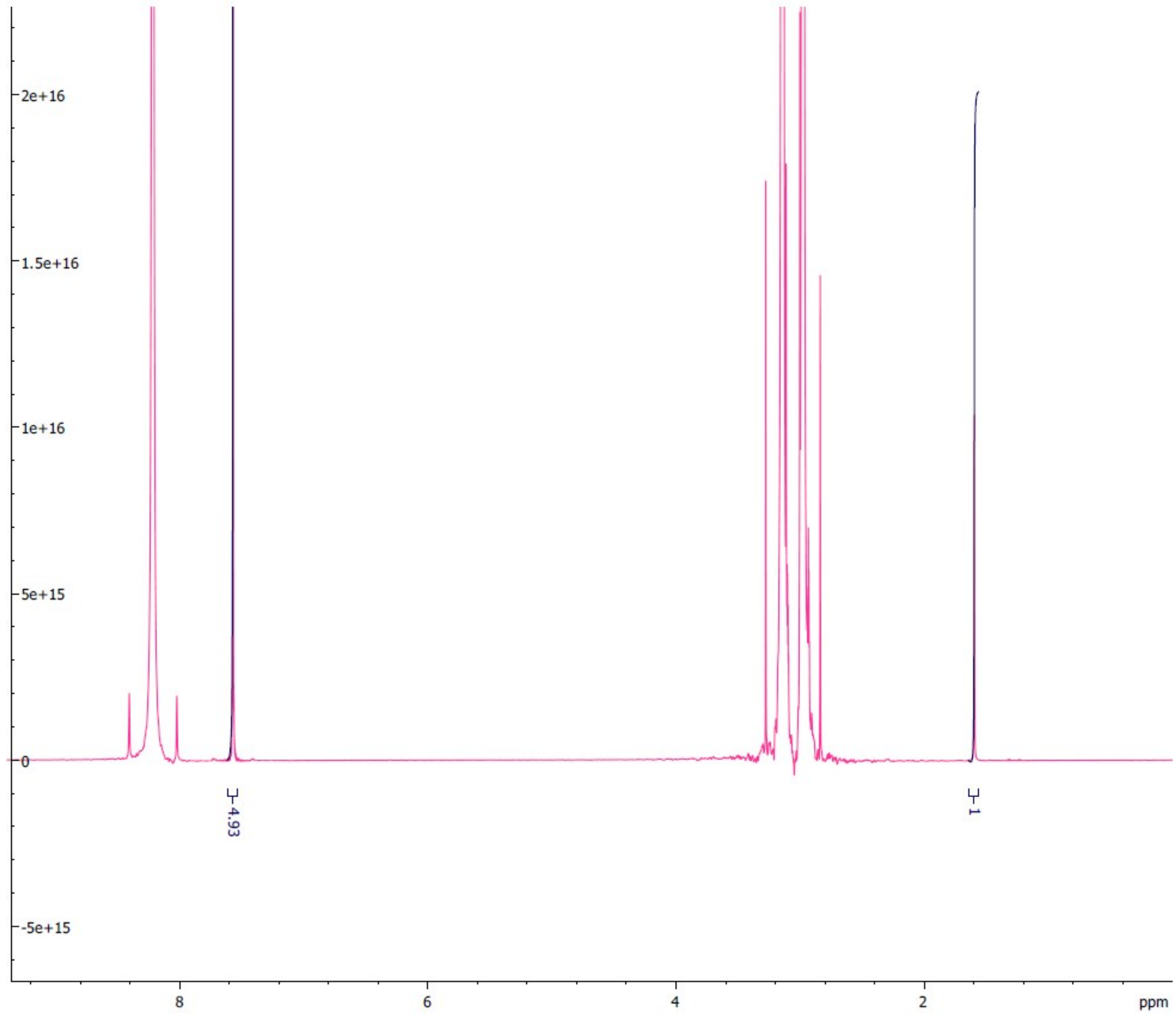

Figure S7. ^{1}H NMR spectrum of a calibration mixture of liquid phase containing 10 µl of benzene and 1 µl of cyclohexane in dimethylformamide/ dimethylformamide-d$_7$.

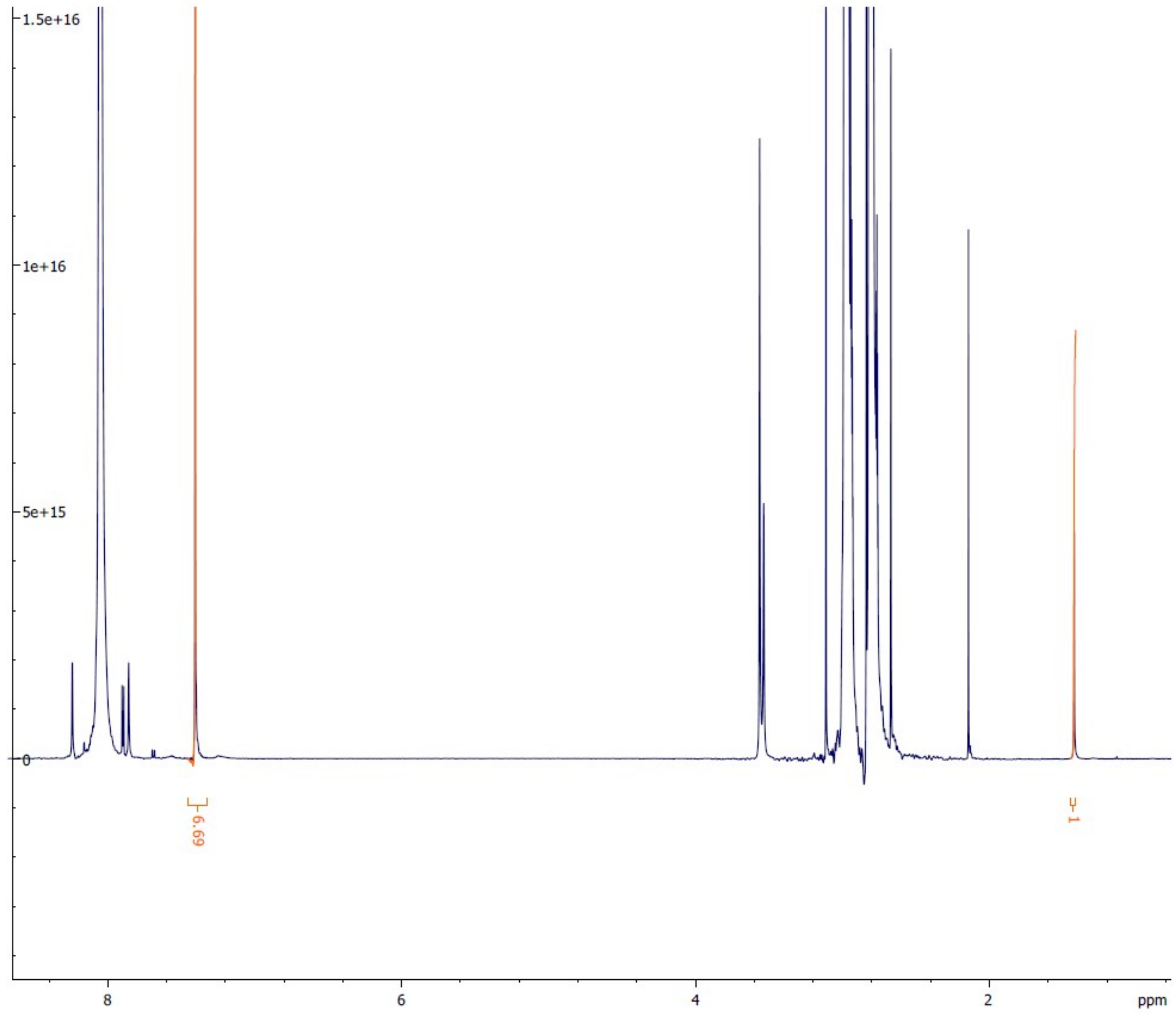

Figure S8. ^{1}H NMR spectrum of the sample after vapor adsorption from 1:1 benzene:cyclohexane mixture. The sample was decomposed with KOH in the liquid phase in dimethylformamide/ dimethylformamide-d_7.

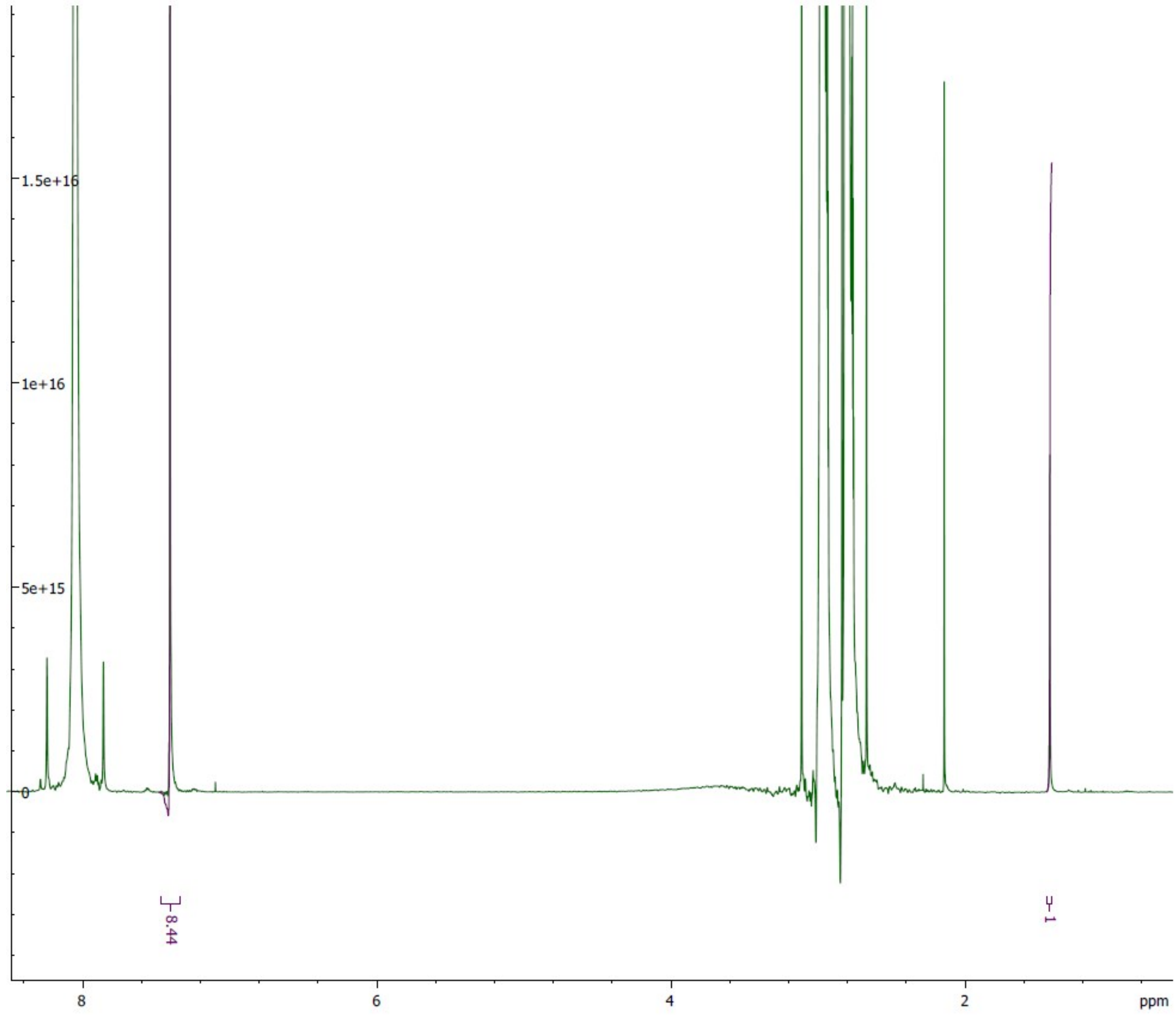

Figure S9. ^{1}H NMR spectrum of the sample after vapor adsorption from 1:1 benzene:cyclohexane mixture. The sample was desorbed with a liquid phase of dimethylformamide/ dimethylformamide-d_7.

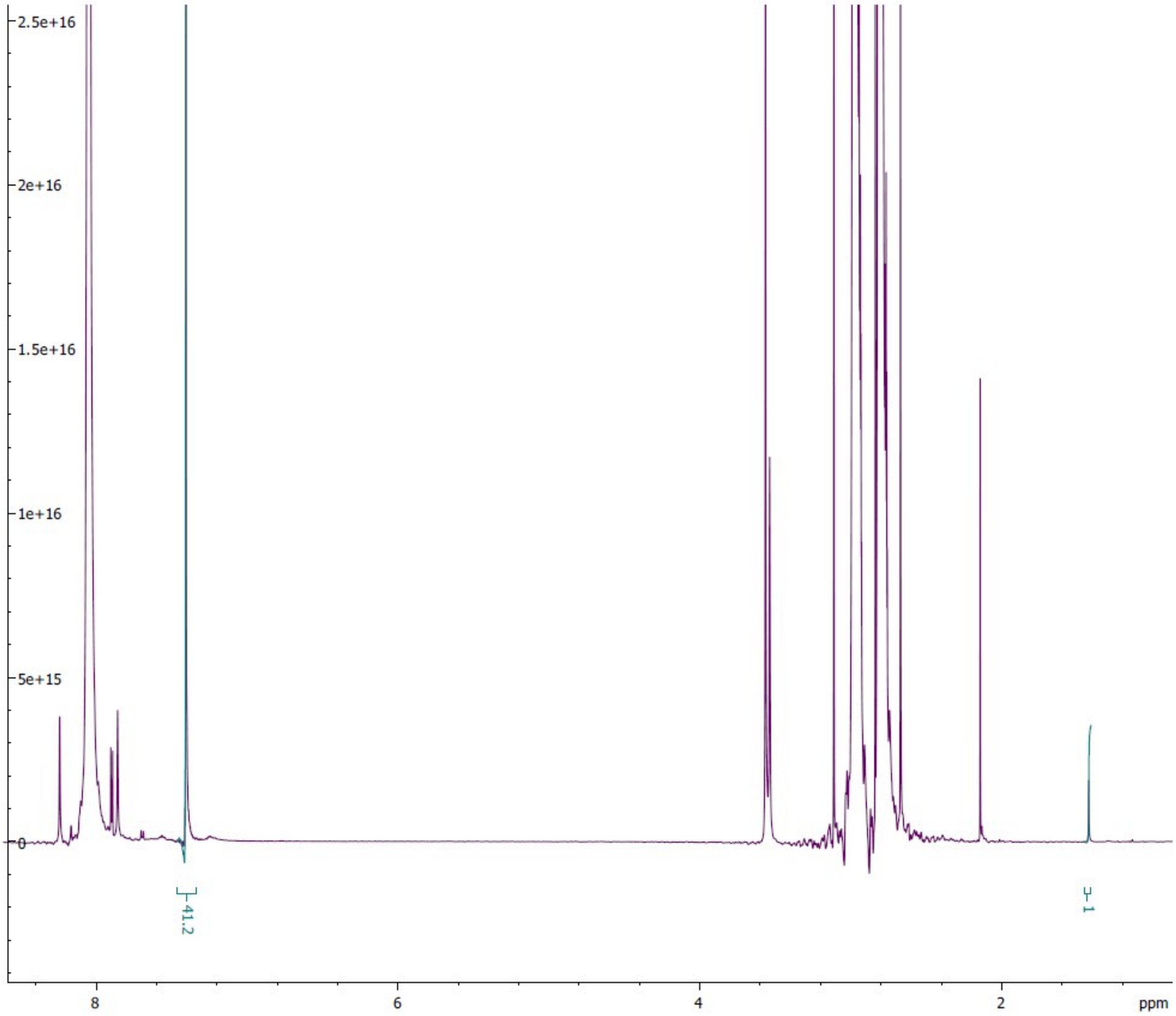

Figure S10. ^{1}H NMR spectrum of the sample after vapor adsorption from 9:1 benzene:cyclohexane mixture. The sample was decomposed with KOH in the liquid phase in dimethylformamide/dimethylformamide-d$_7$.

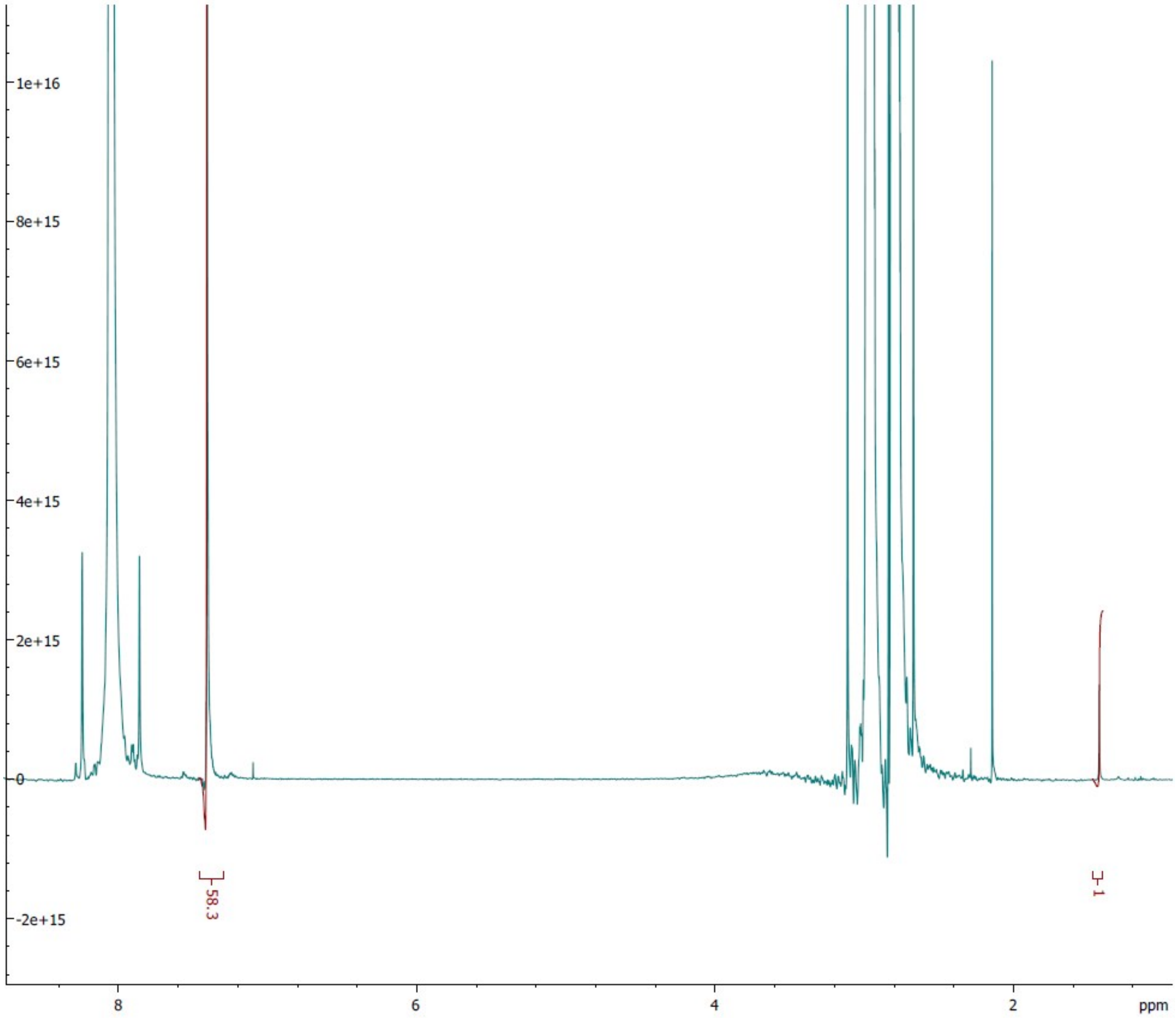

Figure S11. ^{1}H NMR spectrum of the sample after vapor adsorption from 9:1 benzene:cyclohexane mixture. The sample was desorbed with a liquid phase of dimethylformamide/ dimethylformamide-d$_7$.

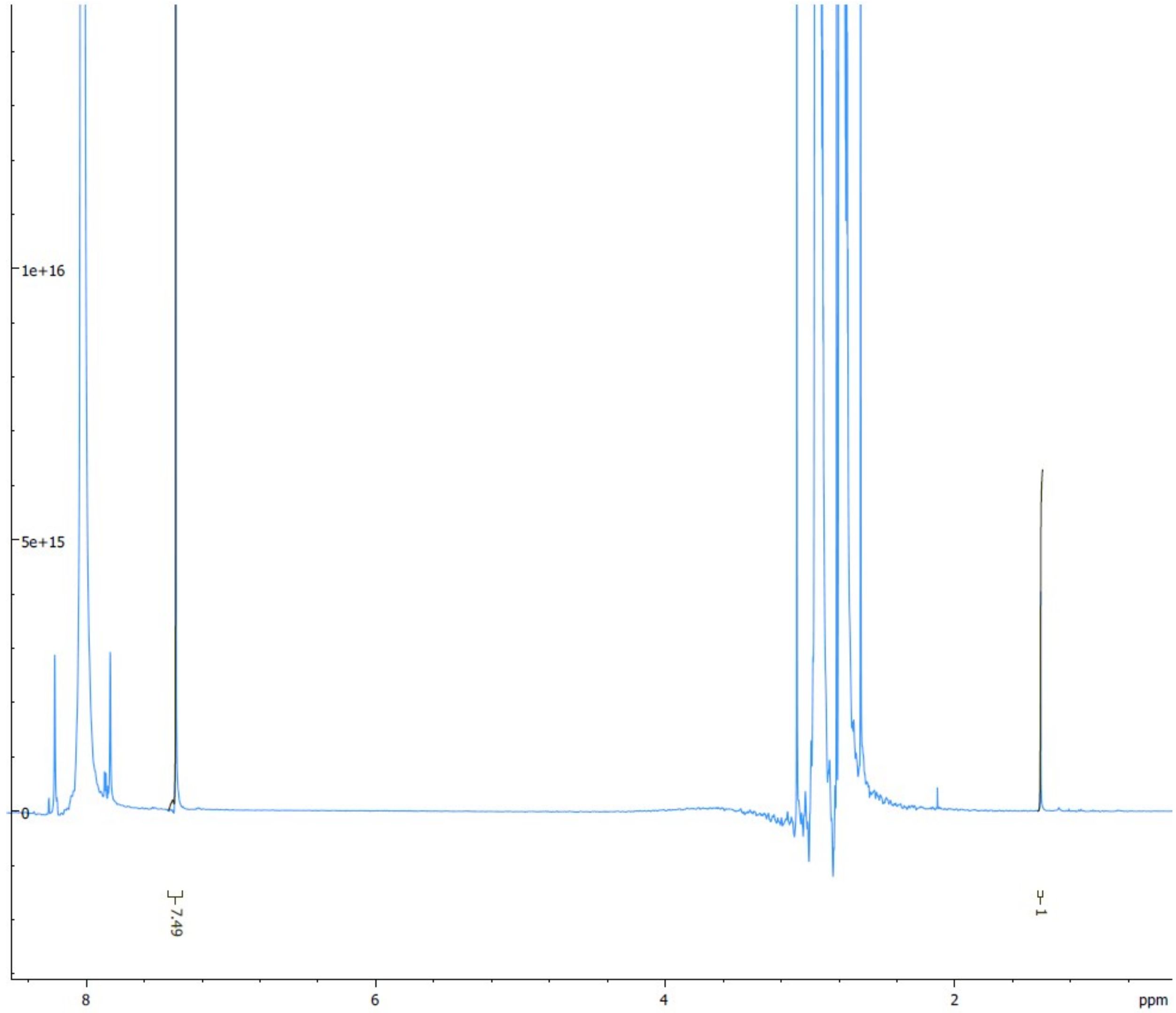

Figure S12. ^{1}H NMR spectrum of the sample after vapor adsorption (20 minutes exposure time) from 1:1 benzene:cyclohexane mixture. The sample was desorbed with a liquid phase of dimethylformamide/ dimethylformamide-d_7.

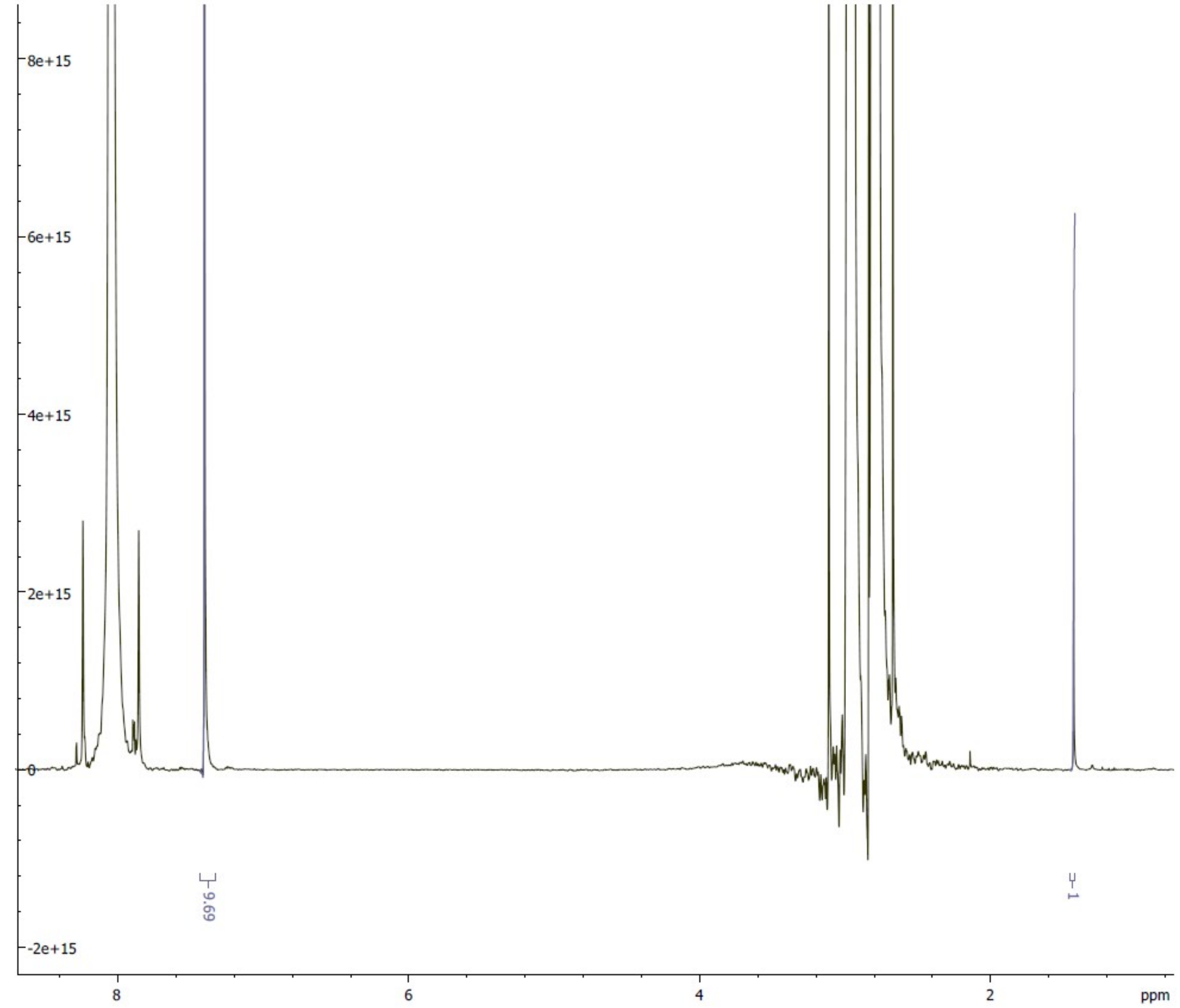

Figure S13. ^{1}H NMR spectrum of the sample after vapor adsorption (150 minutes exposure time) from 1:1 benzene:cyclohexane mixture. The sample was desorbed with a liquid phase of dimethylformamide/ dimethylformamide-d$_7$.

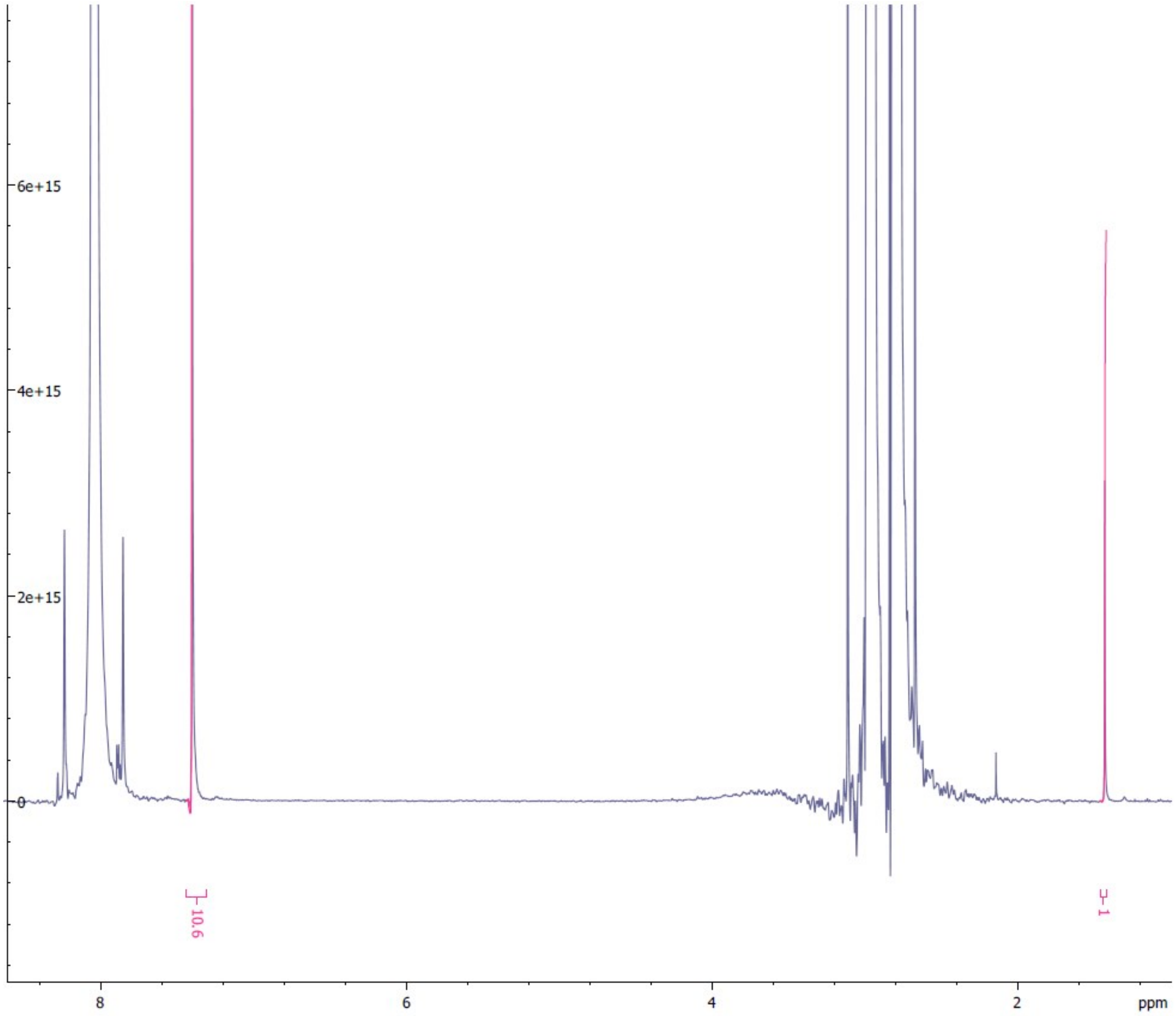

Figure S14. ^{1}H NMR spectrum of the sample after vapor adsorption (1440 minutes exposure time) from 1:1 benzene:cyclohexane mixture. The sample was desorbed with a liquid phase of dimethylformamide/ dimethylformamide-d_7.

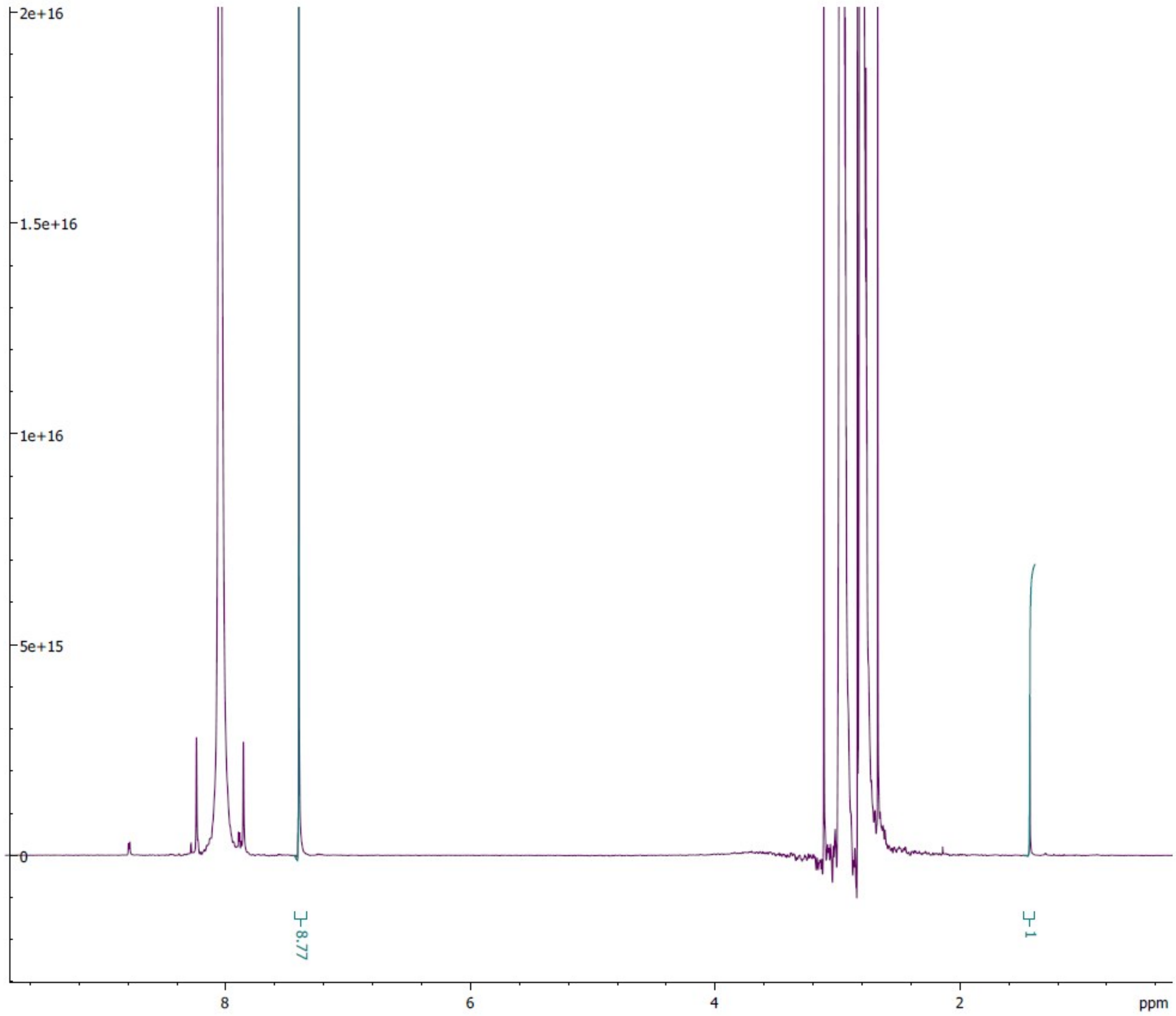

Figure S15. ^{1}H NMR spectrum of the sample after first cycle vapor adsorption (50 minutes exposure time) from 1:1 benzene:cyclohexane mixture. The sample was desorbed with a liquid phase of dimethylformamide/ dimethylformamide-d_7.

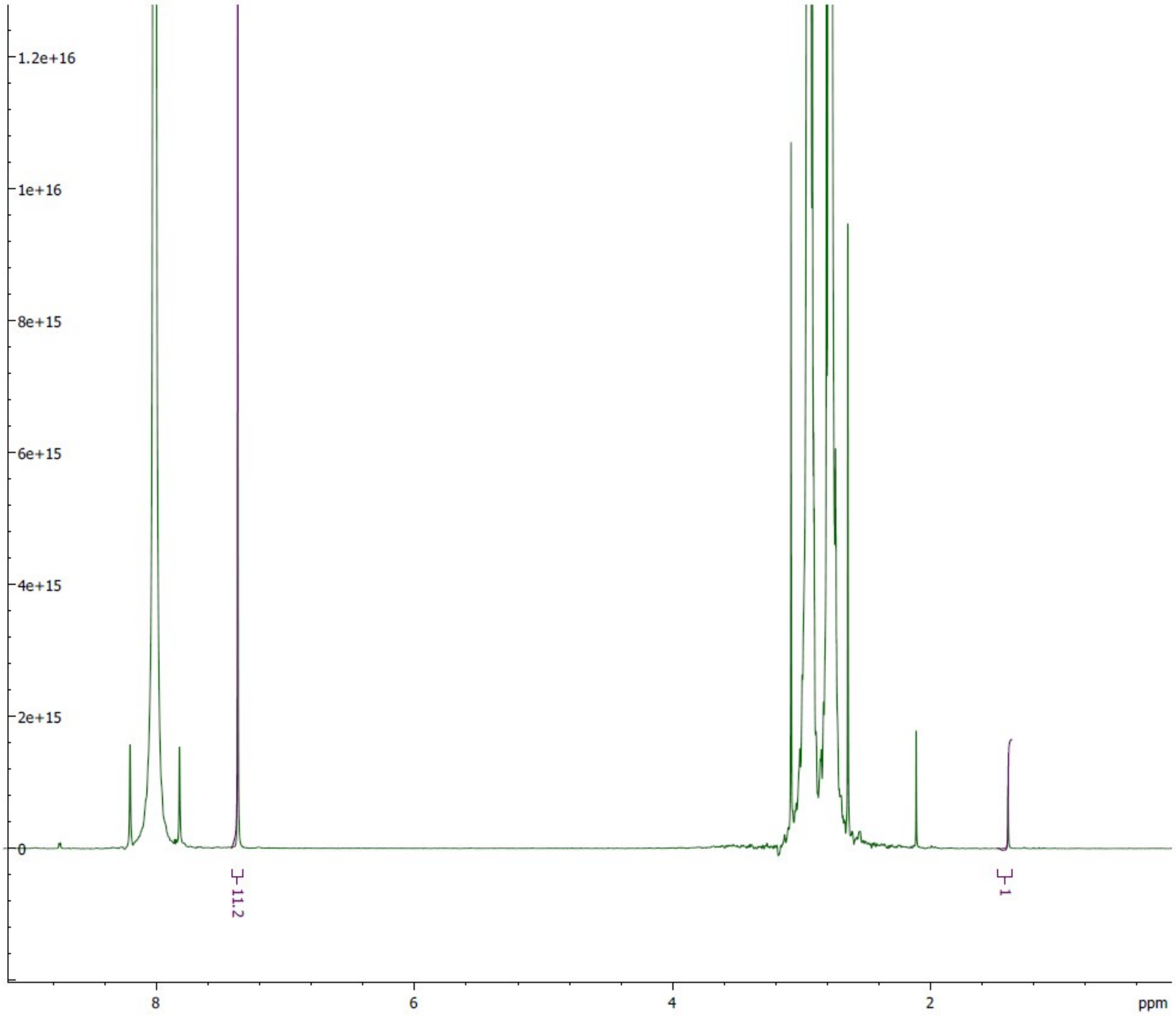

Figure S16. ^{1}H NMR spectrum of the sample after second cycle vapor adsorption (50 minutes exposure time) from 1:1 benzene:cyclohexane mixture. The sample was desorbed with a liquid phase of dimethylformamide/ dimethylformamide-d$_7$.

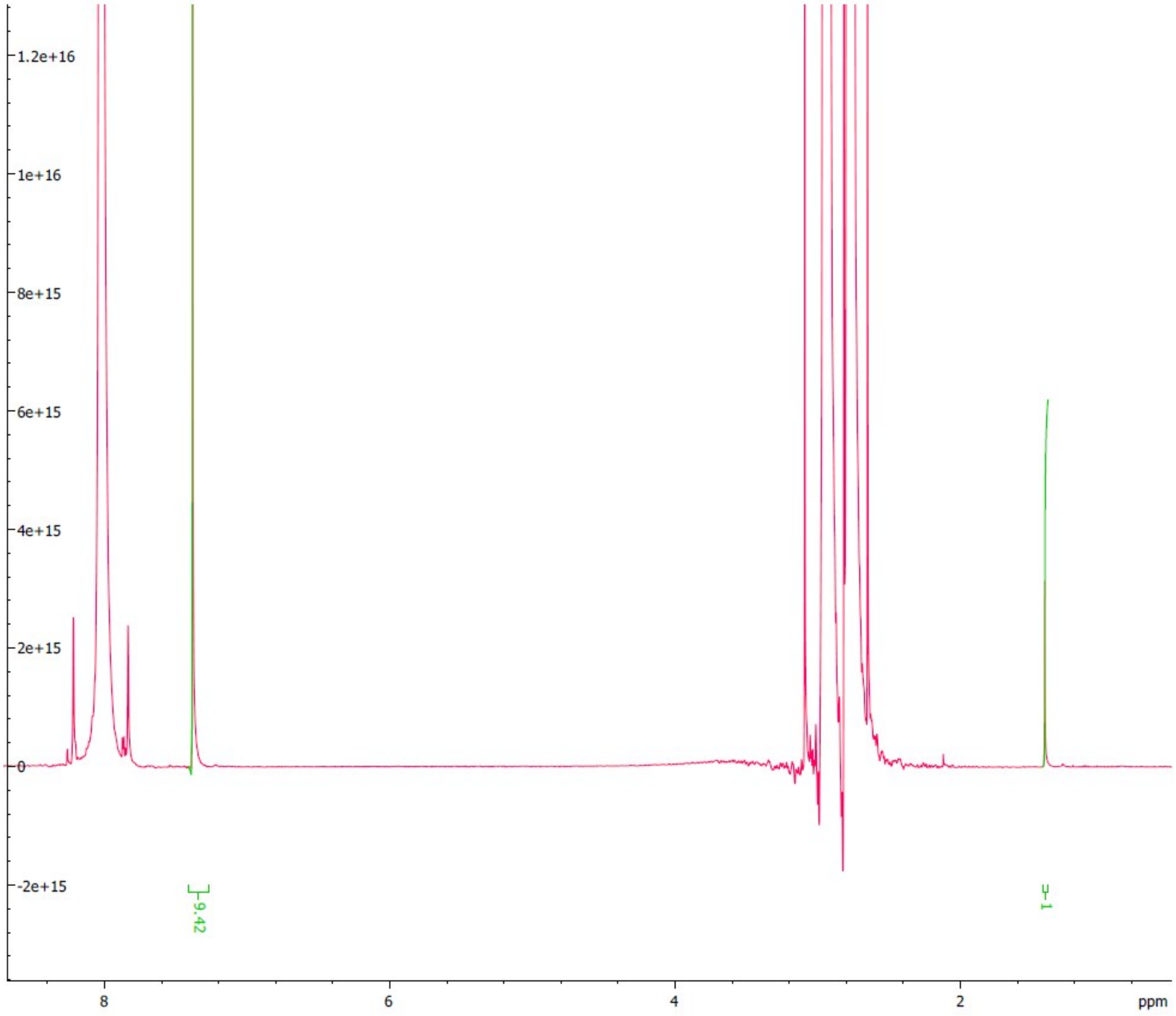

Figure S17. ^{1}H NMR spectrum of the sample after third cycle vapor adsorption (50 minutes exposure time) from 1:1 benzene:cyclohexane mixture. The sample was desorbed with a liquid phase of dimethylformamide/ dimethylformamide-d$_7$.

Table S4. The molar ratio of benzene:cyclohexane in the adsorbed phase after each cycle after vapor separation of an equimolar mixture by activated **1-NO$_2$**.

№ of cycle	Benzene:cyclohexane, %
1	94.6 : 5.4
2	95.7 : 4.3
3	95.0 : 5.0

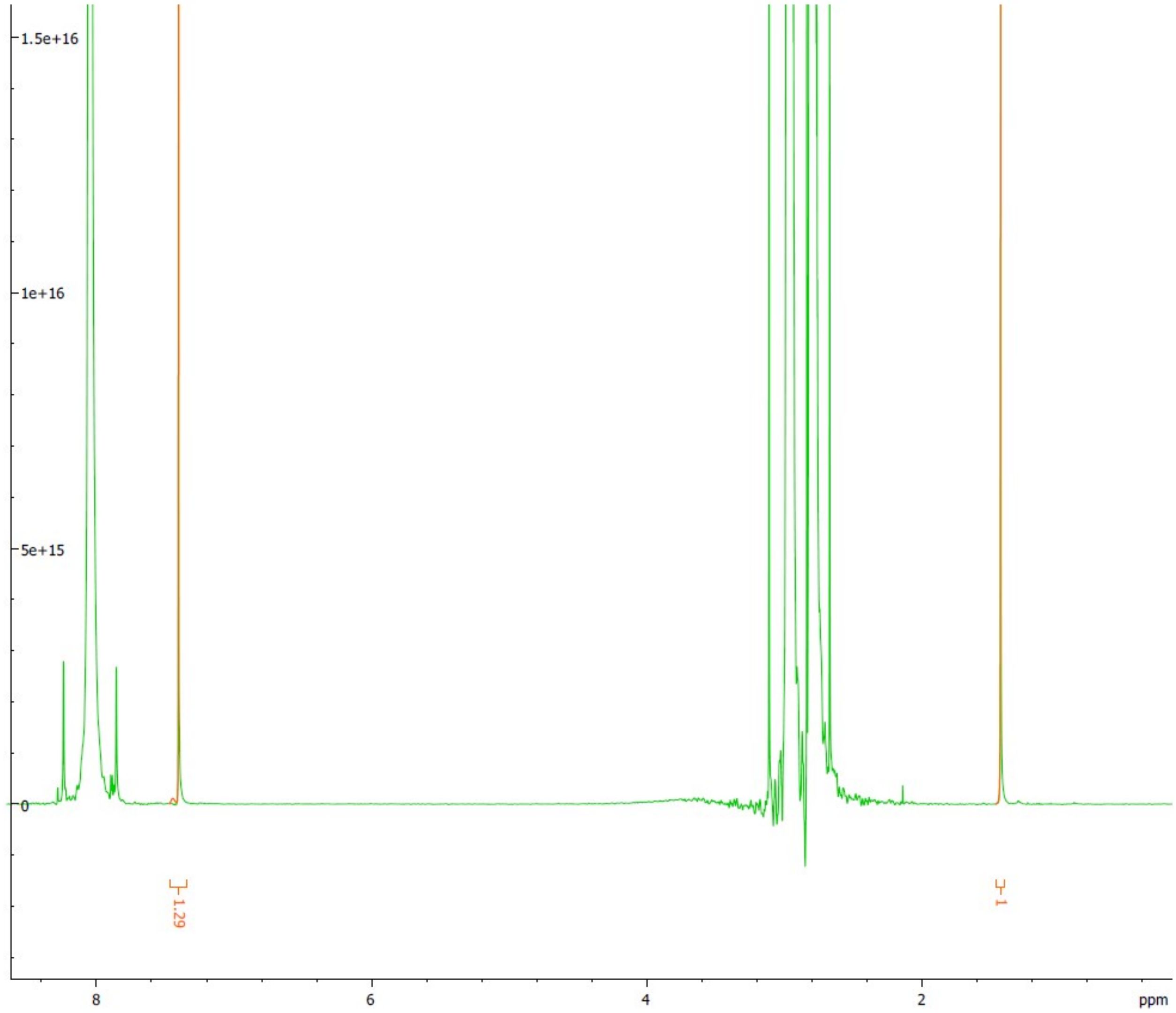

Figure S18. ^{1}H NMR spectrum of the sample after vapor adsorption (50 minutes exposure time) from 1:9 benzene:cyclohexane mixture. The sample was desorbed with a liquid phase of dimethylformamide/ dimethylformamide-d$_7$.

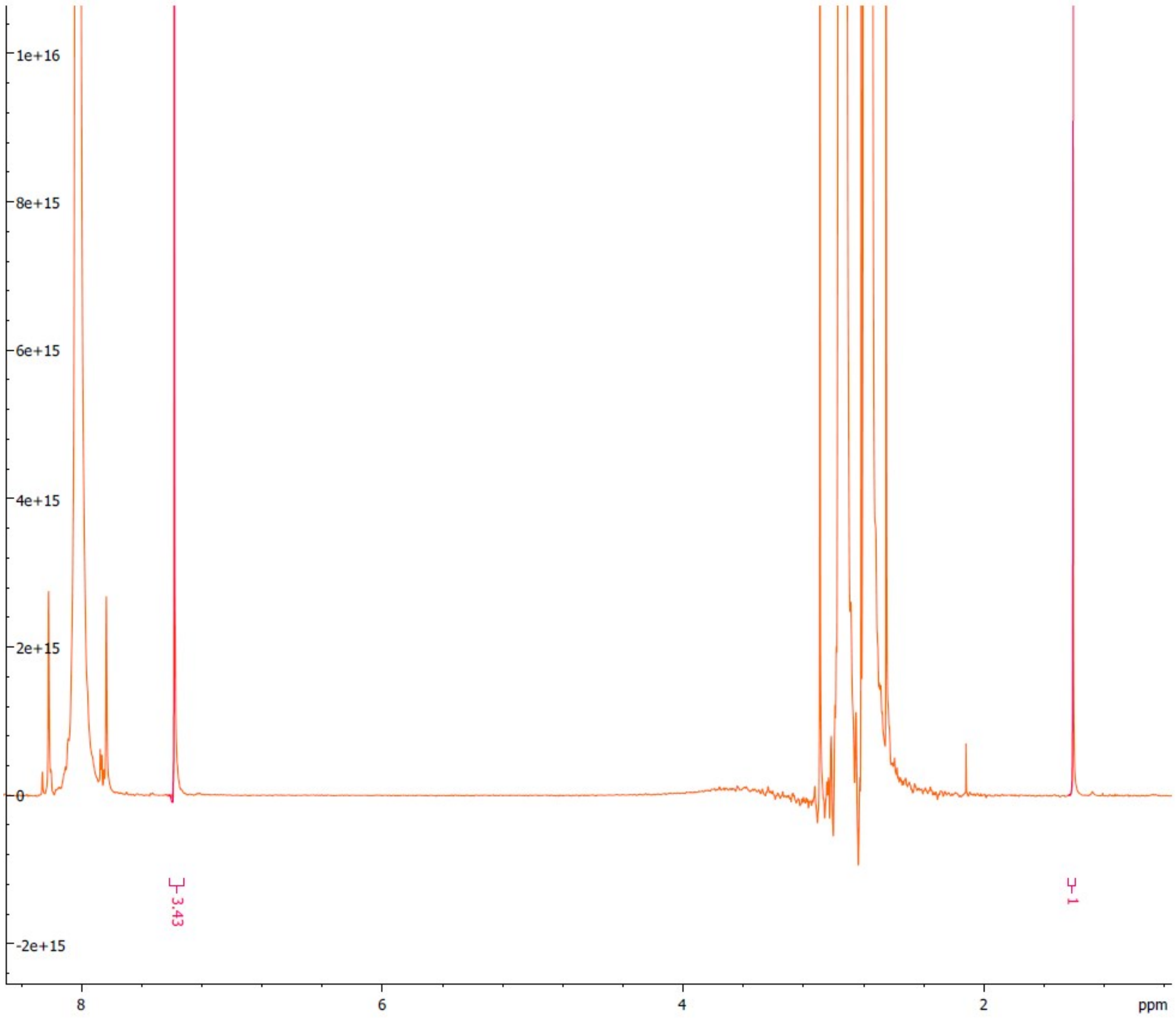

Figure S19. ^{1}H NMR spectrum of the sample after vapor adsorption (50 minutes exposure time) from 1:3 benzene:cyclohexane mixture. The sample was desorbed with a liquid phase of dimethylformamide/ dimethylformamide-d$_7$.

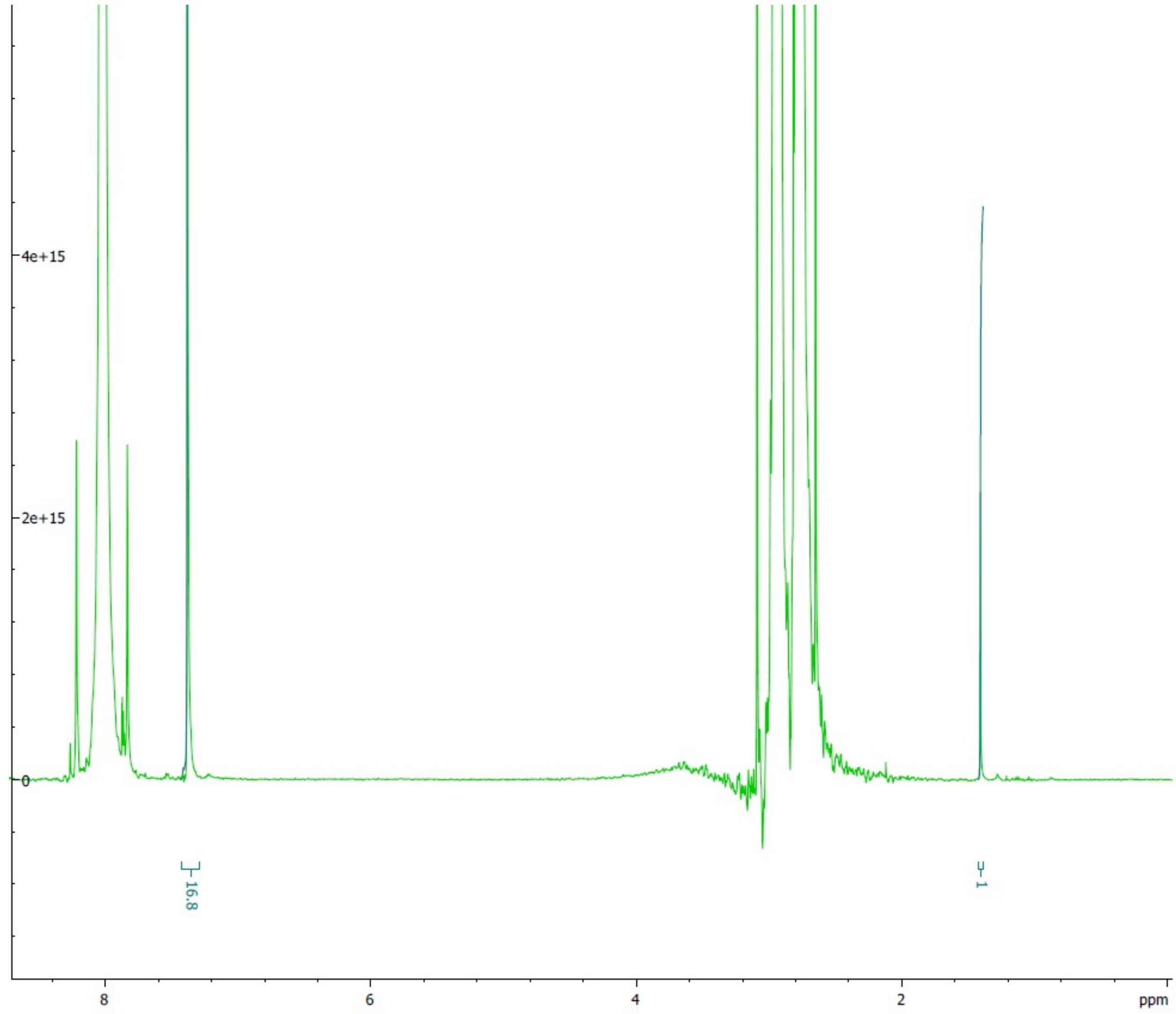

Figure S20. ^{1}H NMR spectrum of the sample after vapor adsorption (50 minutes exposure time) from 3:1 benzene:cyclohexane mixture. The sample was desorbed with a liquid phase of dimethylformamide/ dimethylformamide-d_7.

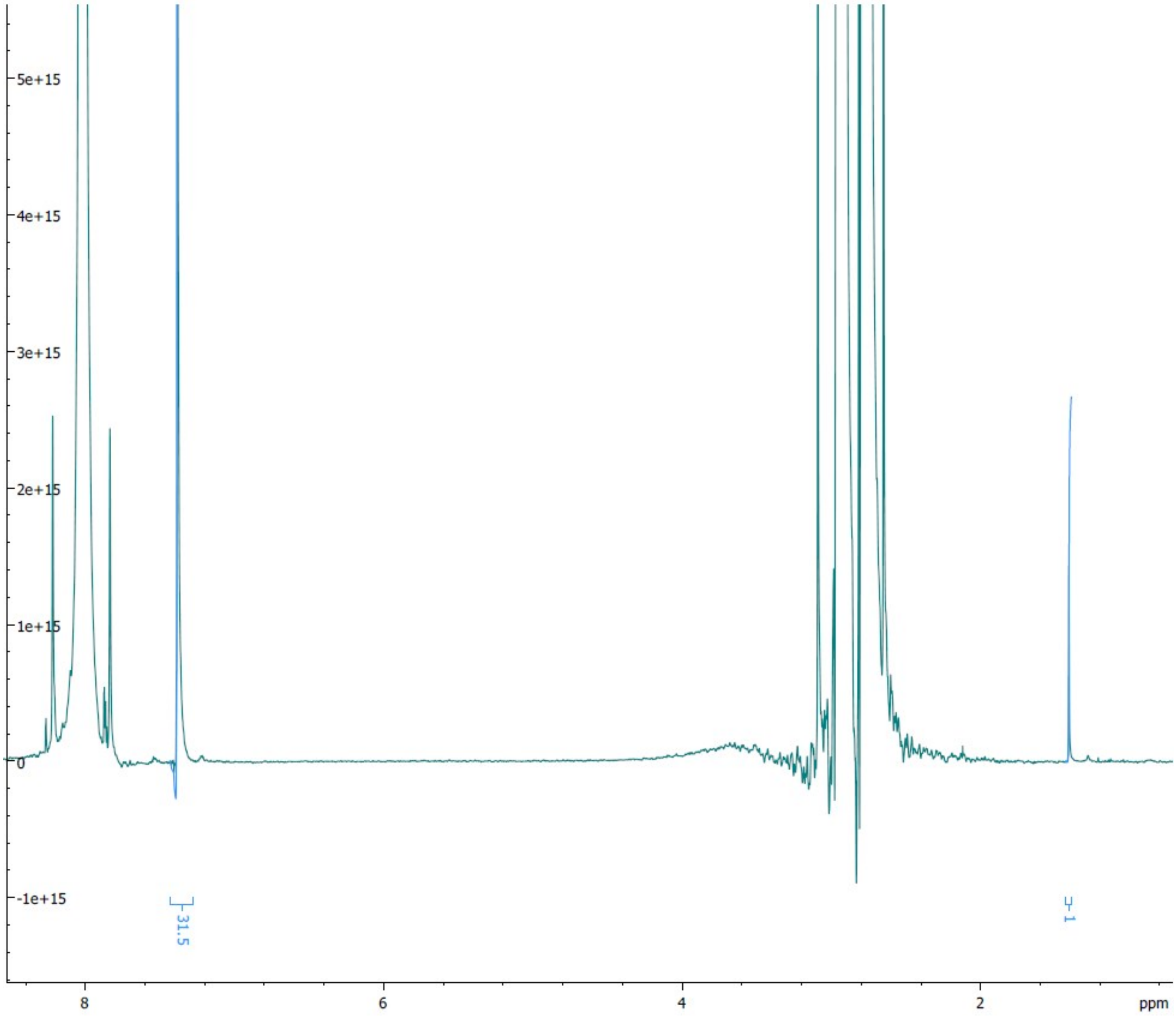

Figure S21. ^{1}H NMR spectrum of the sample after vapor adsorption (50 minutes exposure time) from 9:1 benzene:cyclohexane mixture. The sample was desorbed with a liquid phase of dimethylformamide/ dimethylformamide-d_7.

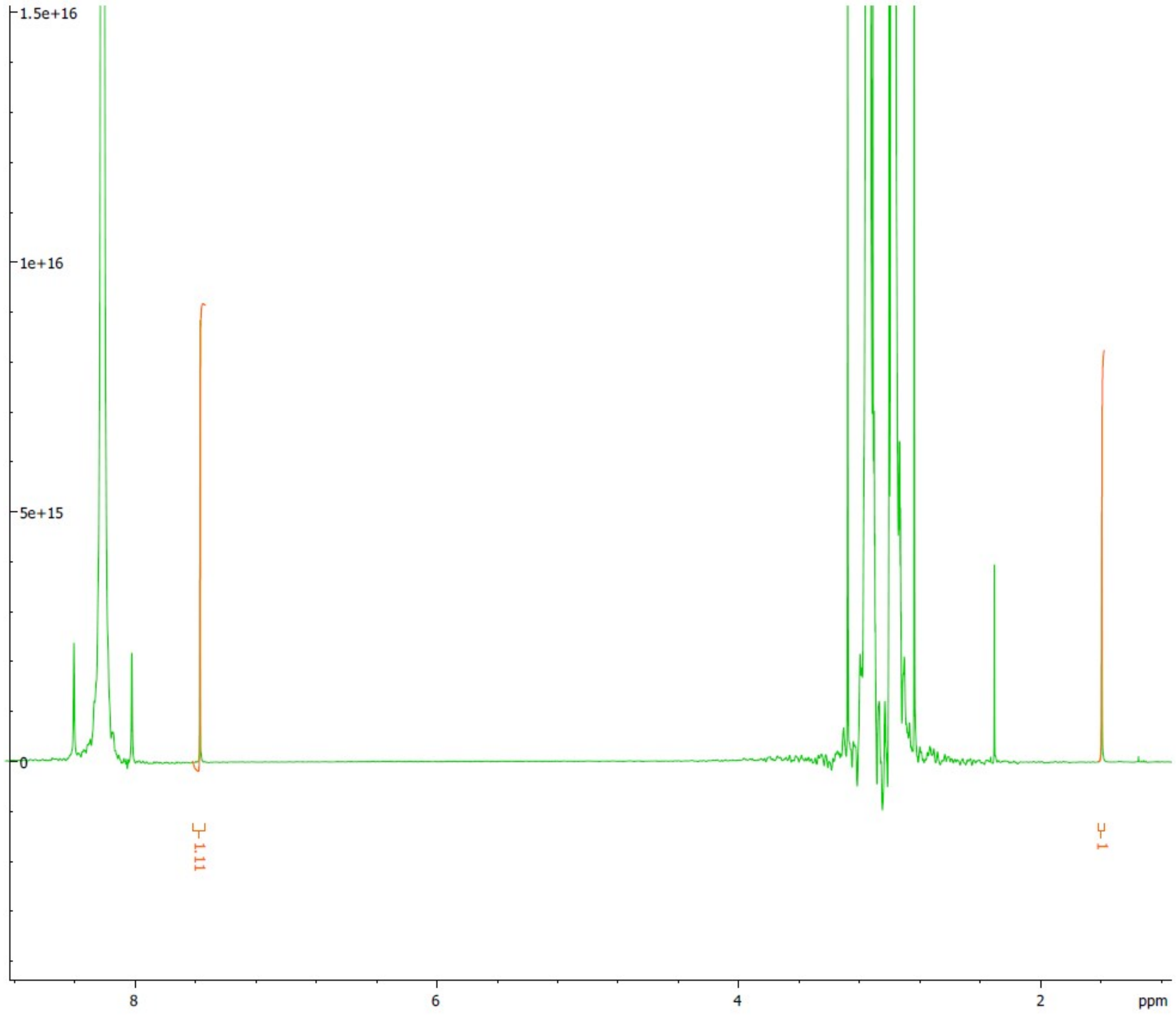

Figure S22. ^{1}H NMR spectrum of the sample after liquid adsorption (1 day exposure time) from 1:9 benzene:cyclohexane mixture. The sample was desorbed with a liquid phase of dimethylformamide/ dimethylformamide-d_7.

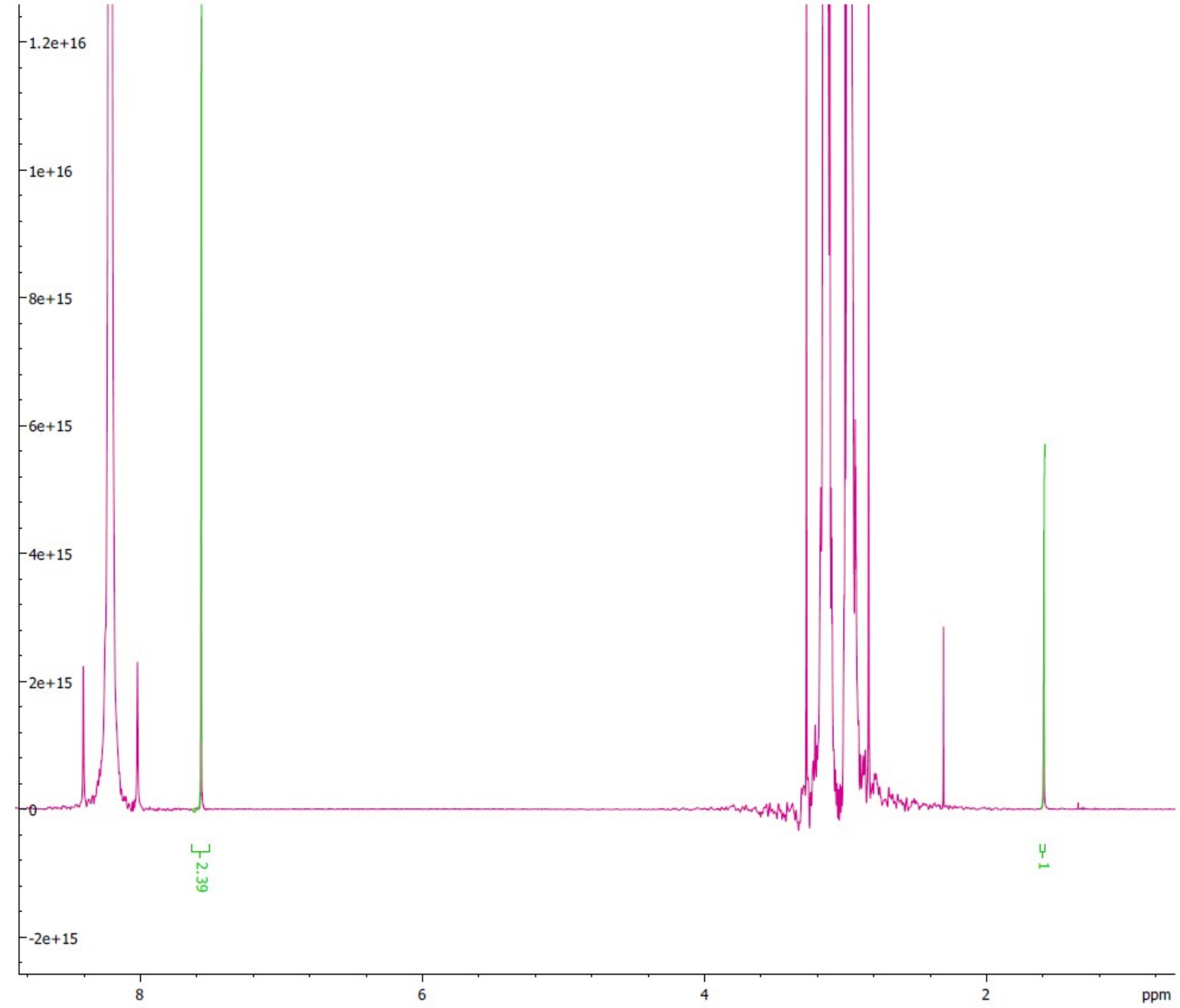

Figure S23. ^{1}H NMR spectrum of the sample after liquid adsorption (1 day exposure time) from 1:3 benzene:cyclohexane mixture. The sample was desorbed with a liquid phase of dimethylformamide/ dimethylformamide-d$_7$.

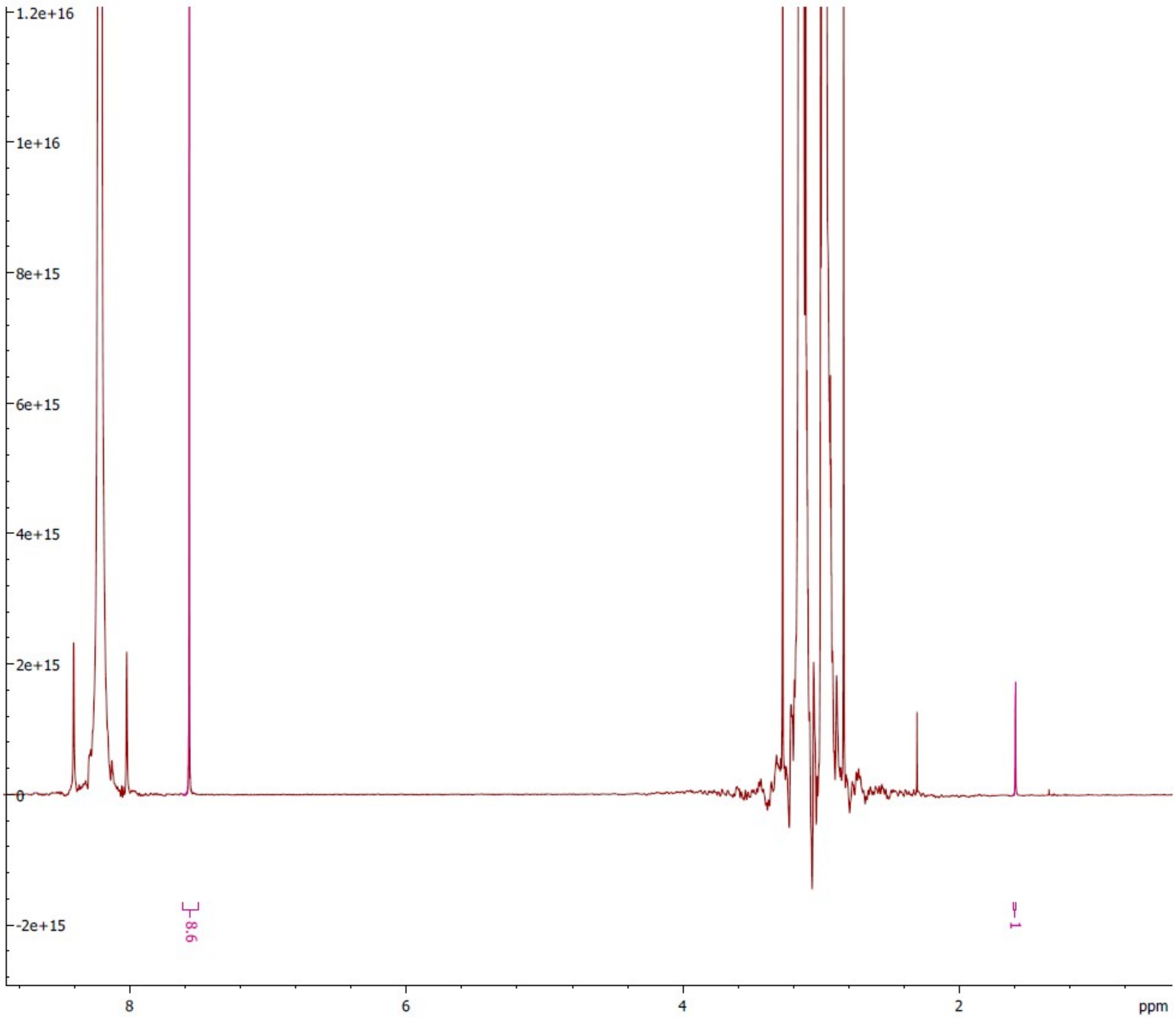

Figure S24. ^{1}H NMR spectrum of the sample after liquid adsorption (1 day exposure time) from 1:1 benzene:cyclohexane mixture. The sample was desorbed with a liquid phase of dimethylformamide/ dimethylformamide-d$_7$.

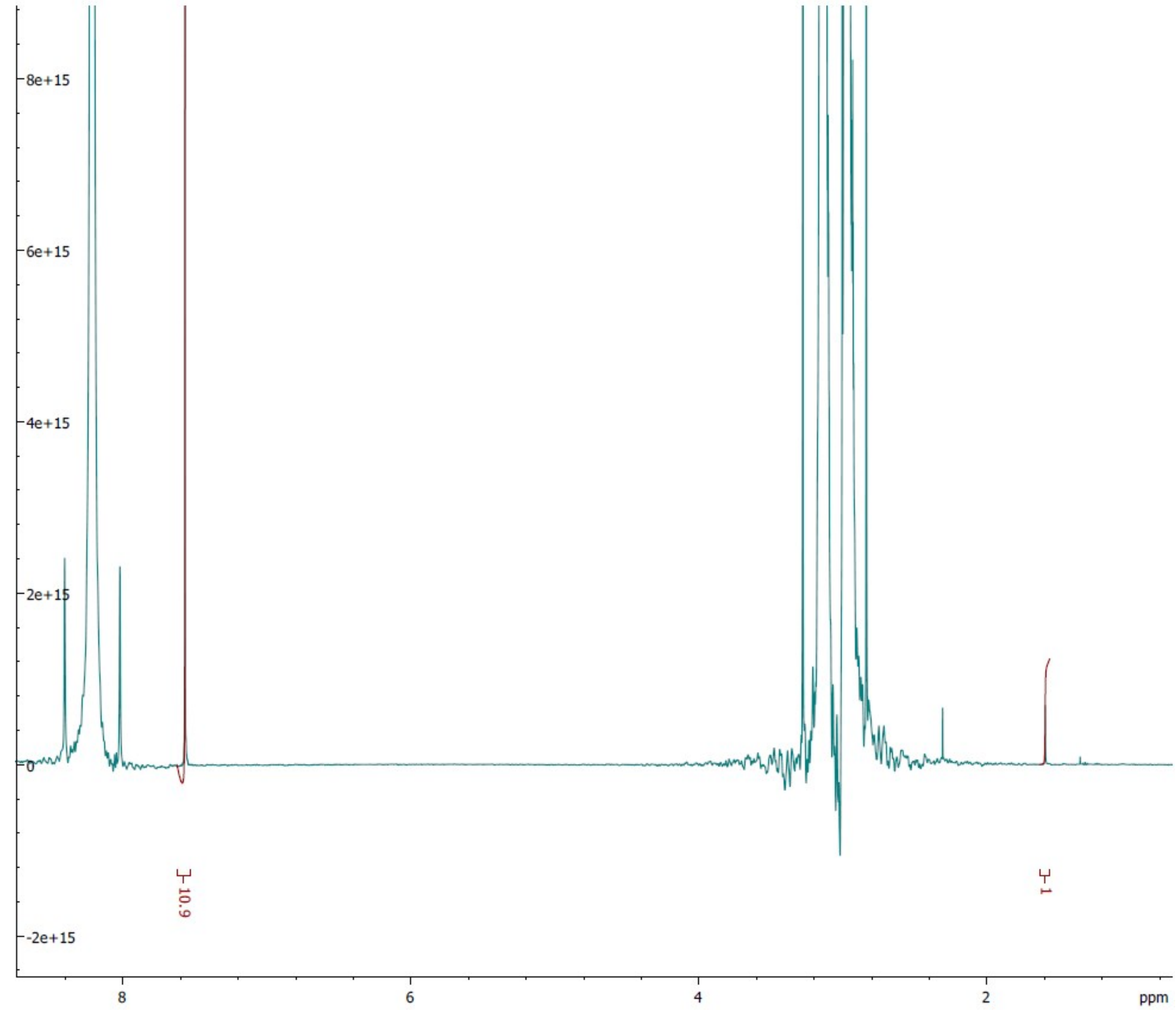

Figure S25. ^{1}H NMR spectrum of the sample after liquid adsorption (1 day exposure time) from 1:3 benzene:cyclohexane mixture. The sample was desorbed with a liquid phase of dimethylformamide/ dimethylformamide-d_7.

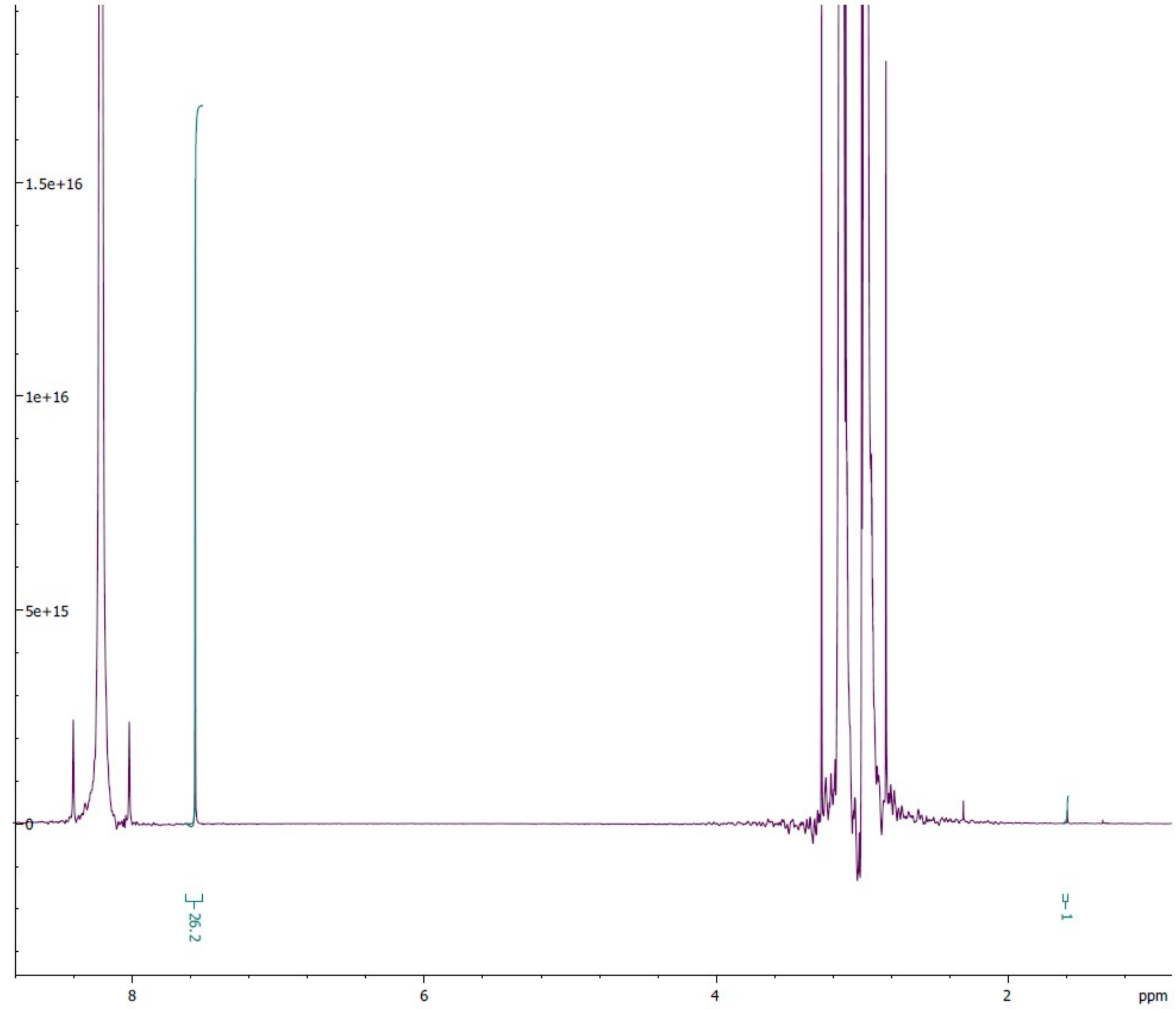

Figure S26. ^{1}H NMR spectrum of the sample after liquid adsorption (1 day exposure time) from 1:9 benzene:cyclohexane mixture. The sample was desorbed with a liquid phase of dimethylformamide/ dimethylformamide-d_7.

Table S5. Benzene/cyclohexane separation from liquid and vapor phases (literature data). The first three examples demonstrate just the highest benzene capacity reported.

Individual benzene and cyclohexane vapor isotherms

MOF	Benzene:cyclohexane selectivity	Max. benzene capacity mmol/g	Reusability	Reference
$[Zn_4O(mptdc)(btb)_{4/3}]$ (H_2mptdc = 3-methyl-4-phenylthieno[2,3-b]thiophene-2,5-dicarboxylic acid)	no data	20.0	no data	7
$[Zn_4O(btb)_2]$	no data	16.8	no data	8
$[Cr_3O(OH)(H_2O)_2(bdc)_3]$	no data	16.7	no data	9
$[Zn(bdc)]$, $[Zn_3(bdc)_3]$, $[Zn_4O(bdc)_3]$	~1:1	10.2	no	10
$[Zn(bdc)(ted)_{0.5}]$	~1:1	6.2	no	11
$[Cu(obb)_2(bpy)_{0.5}(dmf)]$	~1:1	2.2	no	12
$[Cu_2I_2(bttp)_4]$	~2:1	2.6	no	13
$[Cu_3(btc)_2]$, $(C_4H_{12}N)_2[Cu_{12}(btc)_8(H_2O)_{12}][HPW_{12}O_{40}]$, $K_2[Cu_{12}(btc)_8(H_2O)_{12}][HPW_{12}O_{40}]$, $Li_2[Cu_{12}(btc)_8(H_2O)_{12}][HPW_{12}O_{40}]$	~2:1	2.5	no	14
$[Zn_2(L1)_2(dmf)_2]$ (L1 = 2-(6-carboxy(methyl)amino)-1,3,5,7-tetraoxo-6,7-dihydrocyclopenta[f]isoindol-2(1H,3H,5H)- yl)propanoic acid	~3:1	1.3	no	15
$[Ni_3(OH)(ina)_3(bdc)_{1.5}]$	21:1	2.9	no	16
$[Cu(etz)]$	30:1	2.6	no	17
$[Zn(pbda)(dpni)]$	40:1	4.2	no	18
$[Cd(ataia)]$	40:1	2.4	no	19
$((C_2H_5)_4N)_3[In_3(tatb)_4]$	120:1	1.7	no	20

Separation of liquid/vapor mixtures

MOF	Ratio in mixture	Benzene:cyclohexane selectivity	Max. benzene capacity mmol/g	Reusability	Reference
$[Cu(bpp)_2(BF_4)_2]$	liquid (1:1)	~45:1 (individual isotherms), benzene ≈ cyclohexane (separation)	3.1	no	21
$((CH_3)_3NH)[Zn_3(OH)(pzc)_3]$, $((C_2H_5)_3NH)[Zn_3(OH)(pzc)_3]$	liquid (1:1)	$((CH_3)_3NH)[Zn_3(OH)(pzc)_3]$ – 3:1, $((C_2H_5)_3NH)[Zn_3(OH)(pzc)_3]$ – 14:1	no data	no	22
$(NH_4)[Cu_3(\mu_3\text{-}OH)(\mu_3\text{-}4\text{-}carboxylapyrazolato)_3]$, $((C_2H_5)_3NH)[Cu_3(\mu_3\text{-}OH)(\mu_3\text{-}4\text{-}carboxylapyrazolato)3]$, $Li[Cu_3(\mu_3\text{-}OH)(\mu_3\text{-}4\text{-}carboxylapyrazolato)3]$	vapor (1:1)	5:1, 8:1, 12:1 respectively	no data	no	23
$[Zn(tcnqtcnq)(bpy)]$	vapor (1:1)	~4:1 (isotherms), 24:1 (separation)	2.8	yes	24
$[Mn(tcnqtcnq)(bpy)]$	vapor (1:1)	~2:1 (isotherms), 19:1 (separation)	3.5	yes	25
ZnL2 (H_2L2 = (R,R)-(-)-N,N'-bis(3-tert-butyl-5- (4-ethynylpyridyl)salicylidene)-1,2-diaminocyclohexane)	liquid (1:1)	~6:1 (isotherms), 24:1 (separation)	1.5	yes	26

[Zn(ip)(bpa)]	vapor (1:1)	~14 (isotherms), 25:1 (separation)	1.2	no	27
$[Zn_4(EGO_2)_2(tdc)_2(dabco)]$	liquid (1:1), vapor (1:1)	92:1 (liquid), 20:1 (vapor)	no data	no	28
This work	**liquid (1:1),** **vapor (1:1)**	**17:1(liquid),** **~15 (isotherms),** **21:1 (vapor)**	**3.9 (-H)** **2.9 (-NO_2)**	**yes**	

Table S6. The weight percent of benzene and cyclohexane found with NMR spectroscopy at different initial ratios for 50 minutes of vapor exposure time.

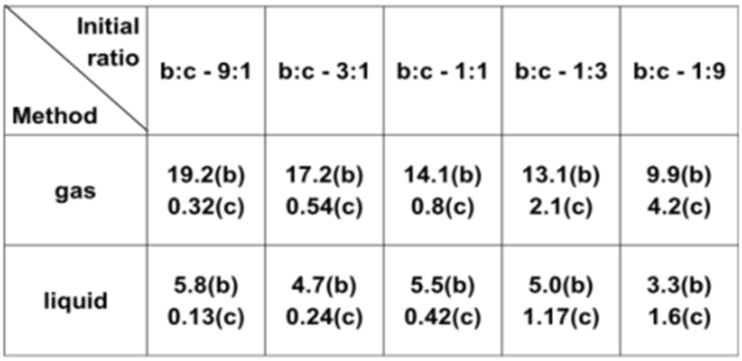

Initial ratio Method	b:c - 9:1	b:c - 3:1	b:c - 1:1	b:c - 1:3	b:c - 1:9
gas	19.2(b) 0.32(c)	17.2(b) 0.54(c)	14.1(b) 0.8(c)	13.1(b) 2.1(c)	9.9(b) 4.2(c)
liquid	5.8(b) 0.13(c)	4.7(b) 0.24(c)	5.5(b) 0.42(c)	5.0(b) 1.17(c)	3.3(b) 1.6(c)

Structure

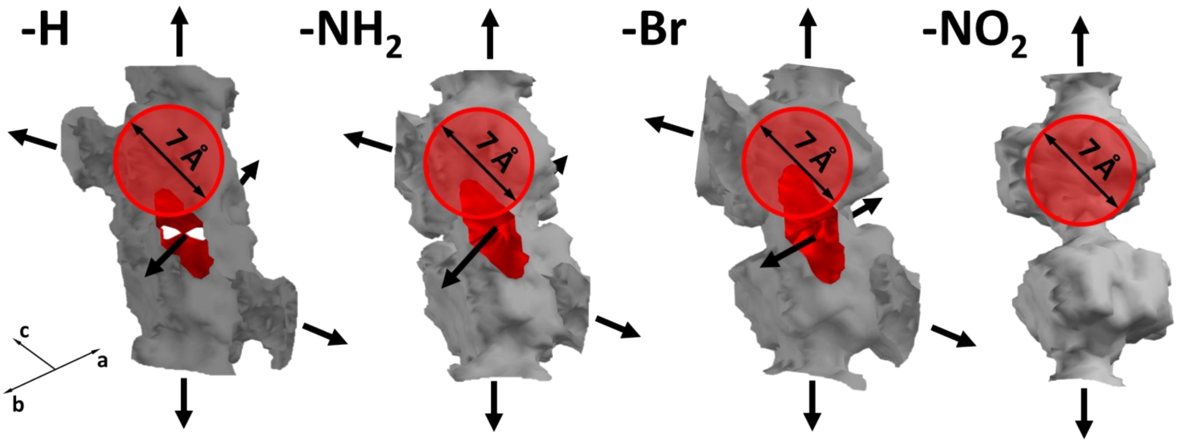

Figure S27. Voids and their connectivity with each other by windows for all 4 compounds

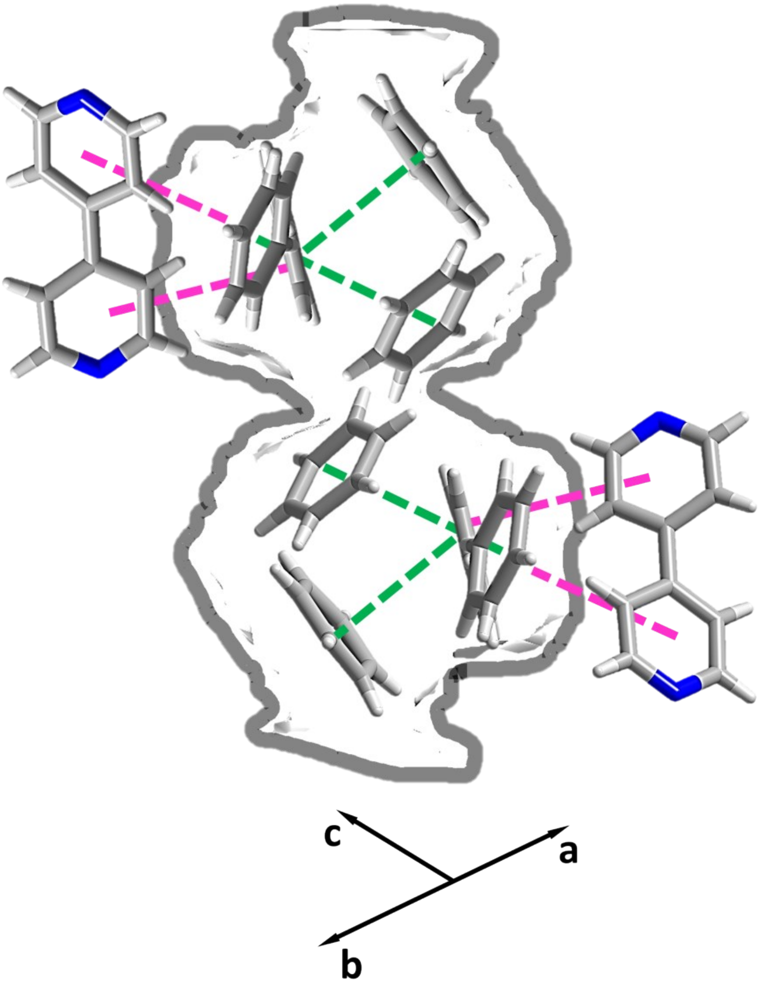

Figure S28. Schematic presentation of the benzene molecule position found in **1-NO$_2$⊃C$_6$H$_6$.** C–H⋯π contacts between host framework and benzene molecules are shown with magenta dashed lines, π–π guest-guest contacts are shown as green dashed lines.

Powder XRD

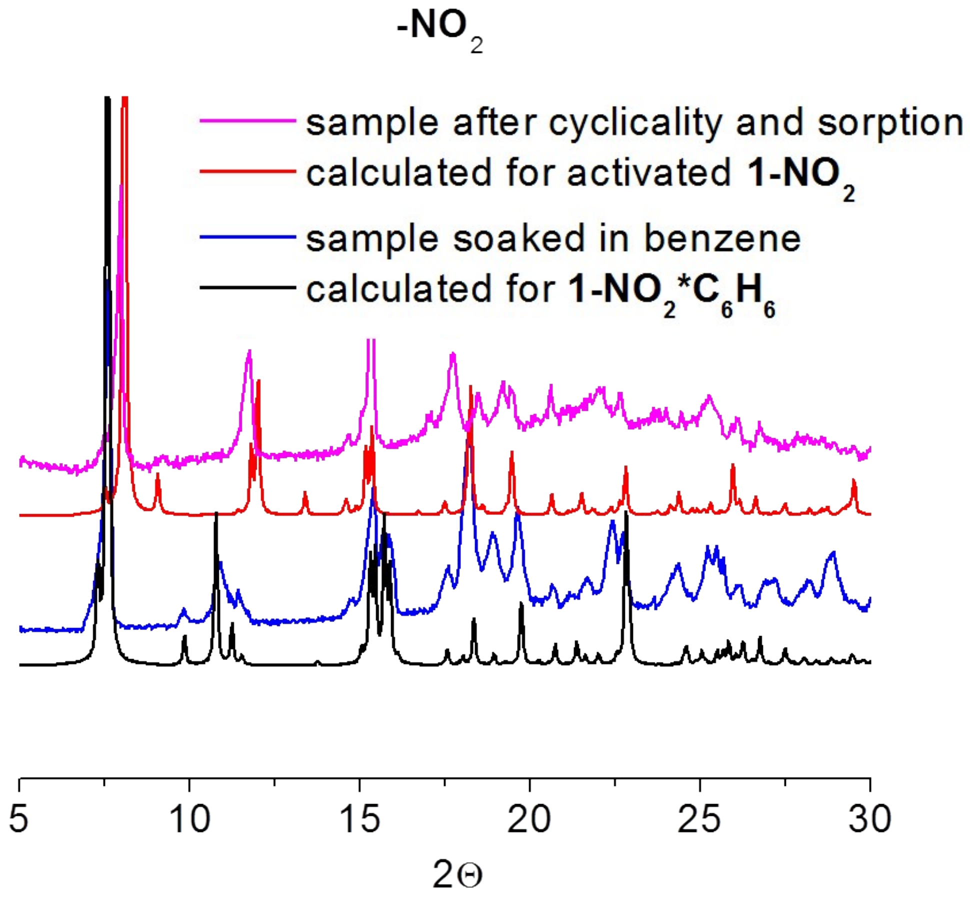

Figure S29. Comparison of experimental PXRD diagrams for **1-NO_2** samples. Magenta – sample was used for 3 cycles of separation of vapor benzene/cyclohexane (1:1), then activated after acetone treatment and used for N_2 sorption experiment at 77 K; red - calculated from SXRD data for sample as synthesized, treated with acetone and then activated; blue - liquid inclusion of benzene; black - **1-$NO_2 \supset C_6H_6$** calculated from synchrotron data.

Three of four compounds demonstrate breathing behavior during gas sorption experiments as was reported earlier [1]. Moreover, even in structure **1-NO_2** (which isotherm has no significant hysteresis loops), if one will compare the structure of the as synthesized framework and framework after activation (without guests), she/he could see signs of the same structural dynamics. In the structure of the activated compound, in the absence of guests, the channels are slightly flattened (Fig. S30). Even such small channel flattering affects on overall structural parameters. Thus, the position of some peaks in the powder diffraction patterns will always vary insignificantly, depending on how much the structure is filled with guest molecules. In the case of a sample soaked in benzene, very good convergence is observed, since all the cavities in the structure are filled, while in the case of the sample after sorption, some discrepancies can be observed, since the framework is not filled with guest molecules (Fig. S29).

The broadening of the peaks is associated with two fundamental factors: firstly, **1-NO_2** crystals exposed to liquid/vapor benzene crack into smaller crystals after each cycle due to the evaporation of benzene, and secondly, the sample preparation procedure to the PXRD experiment involves grinding to obtain a more homogeneous phase. Both of these factors lead to a significant decrease in crystallite size, which in turn should cause the broadening of the peaks in the powder pattern for a real sample in comparison with that calculated from single crystal data (Fig. S29, S31). To prove structural integrity nitrogen sorption isotherms for **1-R (R = H, Br, NH$_2$, NO$_2$)** at 77K after benzene/cyclohexane sorption experiments were carried out (Figure S32). BET data for the corresponding compounds (Table S7) corresponds nicely to the values before benzene/cyclohexane sorption/separation experiments.

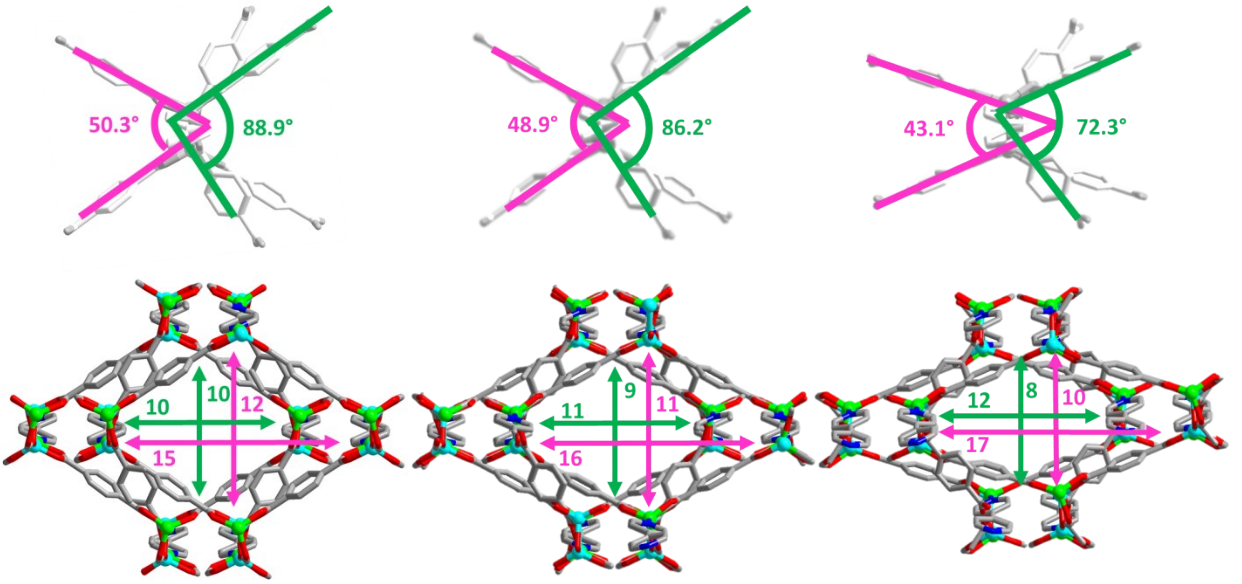

with benzene **as synthesized** **activated**

Figure S30. Channel flattering in **1-NO$_2$⊃C$_6$H$_6$**, **1-NO$_2$** as synthesized and activated (distances are shown in angstroms).

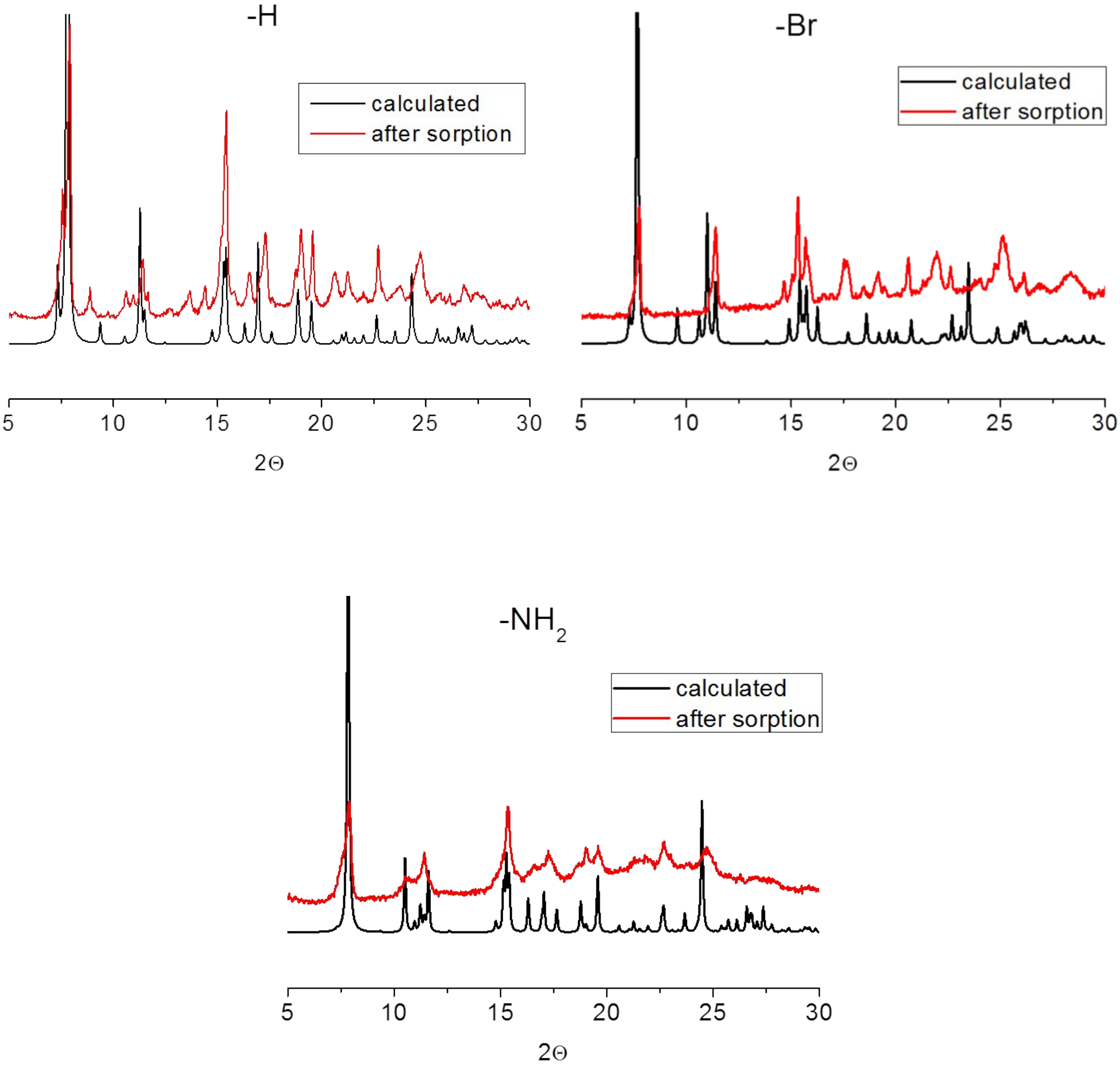

Figure S31. The stability of **1-R** frameworks after vapor sorption experiments. Red – samples of **1-R** after individual component vapor sorption of benzene and cyclohexane; black – calculated from SXRD for as synthesized **1-R**.

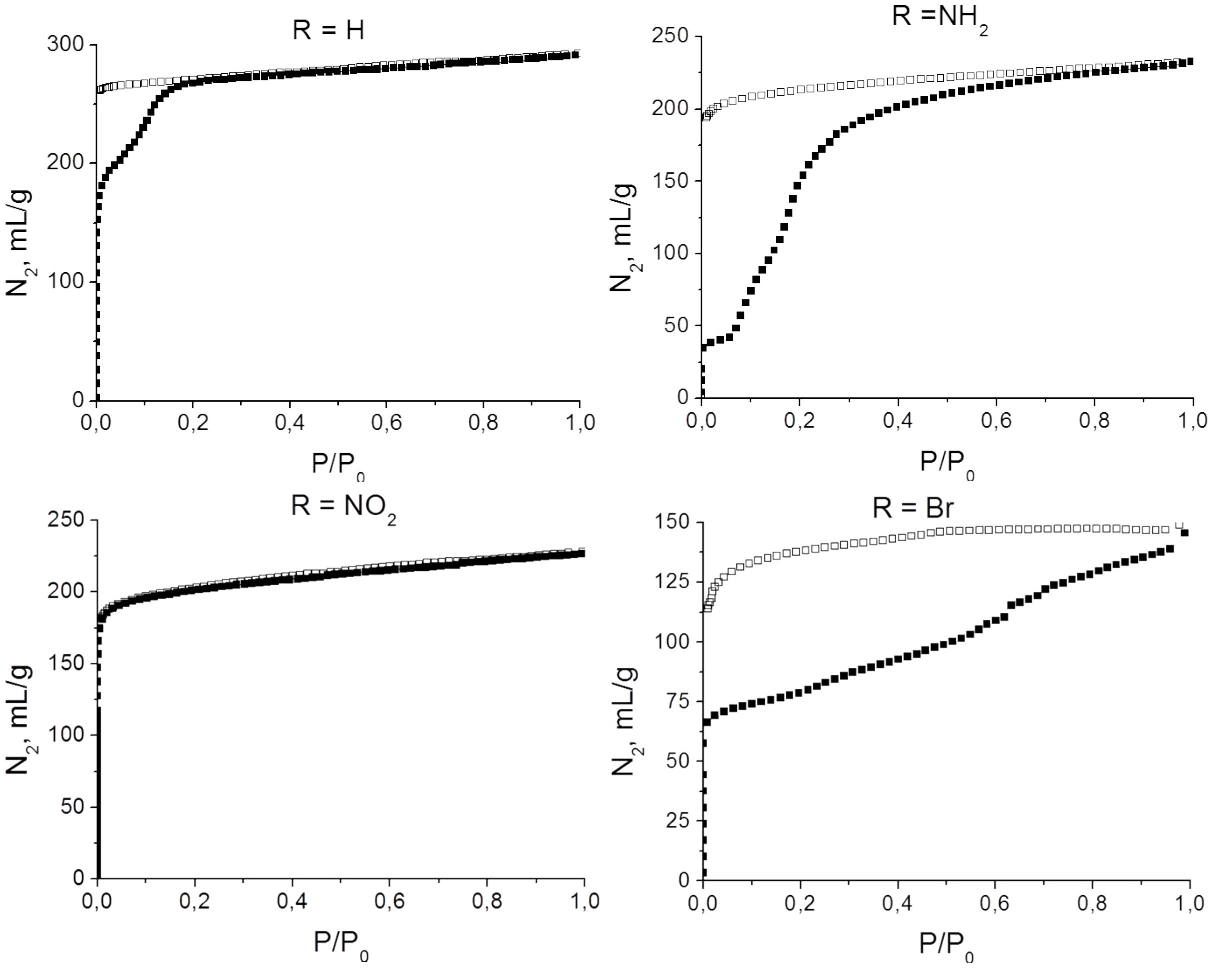

Figure S32. Nitrogen sorption isotherms for 1-R at 77K after benzene/cyclohexane sorption experiments (**1-NO_2** after 3rd cycle, other **1-R** after single components sorption experiments). Adsorption is shown with filled figures, desorption – empty.

Table S7. Comparison of calculated BET surface areas for **1-R** before separation (BET_1) and BET after all sorption/selectivity experiments (BET_2).

Compound	BET_1, $m^2 \cdot g^{-1}$	BET_2, $m^2 \cdot g^{-1}$
1-H	1052	1135
1-NH_2	876	855
1-NO_2	742	800
1-Br	431	446

References

1. Sapianik, A.A.; Zorina-Tikhonova, E.N.; Kiskin, M.A.; Samsonenko, D.G.; Kovalenko, K.A.; Sidorov, A.A.; Eremenko, I.L.; Dybtsev, D.N.; Blake, A.J.; Argent, S.P.; Schröder, M.; Fedin, V.P., Rational Synthesis and Investigation of Porous Metal-Organic Framework Materials from a Preorganized Heterometallic Carboxylate Building Block, Inorg. Chem., 2017, 56, 1599-1608
2. Kabsch, W., XDS. Acta Crystallogr., 2010, D66, 125-132.

3. Sheldrick, G. M., SHELXT – Integrated space-group and crystal-structure determination. Acta Cryst. 2015, A71, 3-8.
4. Sheldrick, G. M., Crystal structure refinement with SHELXL. Acta Cryst. 2015, C71, 3.
5. Thermophysical Properties of Fluid Systems, Database of National Institute of Standards and Technology, NIST. http://webbook.nist.gov/chemistry/fluid/
6. Myers, A.L.; Prausnitz, J.M., Thermodynamics of mixed-gas adsorption, AIChE J., 1965, 11, 121–127.
7. He, W.-W., Yang, G.-S., Tang, Y.-J., Li, S.-L., Zhang, S.-R., Su, Z.-M., Lan, Y.-Q., Phenyl Groups Result in the Highest Benzene Storage and Most Efficient Desulfurization in a Series of Isostructural Metal–Organic Frameworks. Chem. Eur. J. 2015, 21, 9784-9789.
8. Gwardiak, S., Szczęśniak, B., Choma, J., Jaroniec, M., Benzene adsorption on synthesized and commercial metal–organic frameworks. J. Porous. Mater., 2019, 26, 775–783.
9. Jhung, S. H., Lee, J.-H., Yoon, J. W., Serre, C., Férey, G., Chang, J.-S., Microwave Synthesis of Chromium Terephthalate MIL-101 and Its Benzene Sorption Ability. Adv. Mater., 2007, 19, 121-124.
10. Eddaoudi, M.; Li, H.; Yaghi, O.M., Highly Porous and Stable Metal–Organic Frameworks: Structure Design and Sorption Properties. J. Am. Chem. Soc. 2000, 122, 1391-1397.
11. Lee, J. Y.; Olson, D.H.; Pan, L.; Emge, Th.J.; Li, J., Microporous Metal–Organic Frameworks with High Gas Sorption and Separation Capacity. Adv. Funct. Mater. 2007, 17, 1255-1262.
12. Tan, Y.-X.; He, Y.-P.; Zhang, J.; Tuning MOF Stability and Porosity via Adding Rigid Pillars. Inorg. Chem. 2012, 51, 9649-9654.
13. Yang, R.; Li, L.; Xiong, Y.; Li, J.-R.; Zhou, H.-C.; Su, Ch.-Y., Two Robust Porous Metal–Organic Frameworks Sustained by Distinct Catenation: Selective Gas Sorption and Single-Crystal-to-Single-Crystal Guest Exchange. Chem. Asian J. 2010, 5, 2358-2368.
14. Ma, F.-J.; Liu, Sh.-X.; Liang, D.-D.; Ren, G.-J.; Wei, F.; Chen, Y.-G.; Su, G.-M., Adsorption of Volatile Organic Compounds in Porous Metal–Organic Frameworks Functionalized by Polyoxometalates. J. Solid St. Chem. 2011, 184, 3034-3039.
15. Joarder, B.; Mukherjee, S.; Chaudhari, A. K.; Desai, A. V.; Manna, B.; Ghosh, S. K., Guest-Responsive Function of a Dynamic Metal–Organic Framework with a π Lewis Acidic Pore Surface. Chem. Eur. J. 2014, 20, 15303-15308.
16. Ren, G.; Liu, Sh.; Ma, F.; Wei, F.; Tang, Q.; Yang, Y.; Liang, D.; Li, Sh.; Chen, Y., A 9- connected Metal–Organic Framework with Gas Adsorption Properties. J. Mater. Chem. 2011, 21, 15909-15913.
17. Zhang, J.-P.; Chen, X.-M., Exceptional Framework Flexibility and Sorption Behavior of a Multifunctional Porous Cuprous Triazolate Framework. J. Amer. Chem. Soc. 2008, 130, 6010-6017.
18. Mukherjee, S.; Babarao, R.; Desai, A. V.; Manna, B.; Ghosh, S. K., Polar Pore Surface Guided Selective CO 2 Adsorption in a Prefunctionalized Metal–Organic Framework. Cryst. Growth Des. 2017, 17, 3581-3587.
19. Das, P.; Mandal, S. K., Strategic Design and Functionalization of an Amine-decorated Luminescent Metal Organic Framework for Selective Gas/Vapor Sorption and Nanomolar Sensing of 2,4,6-Trinitrophenol in Water. ACS Appl. Mater. Interfaces 2018, 10, 25360– 25371.
20. Huang, Y.; Lin, Z.; Fu, H.; Wang, F.; Shen, M.; Wang, X.; Cao, R., Porous Anionic Indium–Organic Framework with Enhanced Gas and Vapor Adsorption and Separation Ability. ChemSusChem 2014, 7, 2647-2653.

21. Kondo, A.; Suzuki, T.; Kotani, R.; Maeda, K., Liquid/Vapor-Induced Reversible Dynamic Structural Transformation of a Three-Dimensional Cu-based MOF to a One-Dimensional MOF Showing Gate Adsorption. Dalton Trans. 2017, 46, 6762-6768.
22. Wang, J.-H.; Luo, D.; Li, M.; Li, D., Local Deprotonation Enables Cation Exchange, Porosity Modulation, and Tunable Adsorption Selectivity in a Metal–Organic Framework. Cryst. Growth Des. 2017, 17, 3387-3394.
23. Quartapelle Procopio, E.; Linares, F.; Montoro, C.; Colombo, V.; Maspero, A.; Barea, E.; Navarro, J. A. R., Cation-Exchange Porosity Tuning in Anionic Metal–Organic Frameworks for the Selective Separation of Gases and Vapors and for Catalysis. Angew. Chem. Int. Ed. 2010, 49, 7308-7311.
24. Shimomura, S.; Horike, S.; Matsuda, R.; Kitagawa, S., Guest-Specific Function of a Flexible Undulating Channel in a 7,7,8,8-Tetracyano-p-quinodimethane Dimer-Based Porous Coordination Polymer. J. Amer. Chem. Soc. 2007, 129, 10990-10991.
25. Shimomura, S.; Matsuda, R.; Kitagawa, S., Flexibility of Porous Coordination Polymers Strongly Linked to Selective Sorption Mechanism. Chem. Mater. 2010, 22, 4129-4131.
26. Li, G.; Zhu, Ch., Xi, X.; Cui, Y., Selective Binding and Removal of Organic Molecules in a Flexible Polymeric Material with Stretchable Metallosalen Chains. Chem. Comm. 2009, 2118-2120.
27. Hijikata, Y.; Horike, S.; Sugimoto, M.; Sato, H.; Matsuda, R.; Kitagawa, S., Relationship between Channel and Sorption Properties in Coordination Polymers with Interdigitated Structures. Chem. Eur. J. 2011, 17, 5138-5144.
28. Lysova, A.A.; Samsonenko, D.G.; Dorovatovskii, P.V.; Lazarenko, V.A.; Khrustalev, V.N.; Kovalenko, K.A.; Dybtsev, D.N.; Fedin, V.P., Tuning the Molecular and Cationic Affinity in a Series of Multifunctional Metal–Organic Frameworks Based on Dodecanuclear Zn(II) Carboxylate Wheels J. Am. Chem. Soc. 2019, 141, 17260-17269.